



HAL
open science

An activity model for phase equilibria in the H₂O-CO₂-NaCl system

Benoît Dubacq, Mike J. Bickle, Katy A. Evans

► **To cite this version:**

Benoît Dubacq, Mike J. Bickle, Katy A. Evans. An activity model for phase equilibria in the H₂O-CO₂-NaCl system. *Geochimica et Cosmochimica Acta*, 2013, 110, pp.229-252. 10.1016/j.gca.2013.02.008 . hal-00817855

HAL Id: hal-00817855

<https://hal.science/hal-00817855>

Submitted on 25 Apr 2013

HAL is a multi-disciplinary open access archive for the deposit and dissemination of scientific research documents, whether they are published or not. The documents may come from teaching and research institutions in France or abroad, or from public or private research centers.

L'archive ouverte pluridisciplinaire **HAL**, est destinée au dépôt et à la diffusion de documents scientifiques de niveau recherche, publiés ou non, émanant des établissements d'enseignement et de recherche français ou étrangers, des laboratoires publics ou privés.

An activity model for phase equilibria in the H₂O-CO₂-NaCl system

Benoît Dubacq^{a,b,*}, Mike J. Bickle^a, Katy A. Evans^c

^a*Dept. of Earth Sciences, Univ. of Cambridge, Downing Street, Cambridge, CB2 3EQ, UK*

^b*ISTeP, UMR 7193, UPMC, Univ. Paris 06, CNRS, F-75005 Paris, France*

^c*Dept. Applied Geology, Curtin Univ. of Technology, GPO Box U1987 Perth, WA 6845, Australia*

Abstract

We present a semi-empirical thermodynamic model with uncertainties that encompasses the full range of compositions in H₂O-CO₂-NaCl mixtures in the range of 10-380°C and 1-3500 bars. For binary H₂O-CO₂ mixtures, the activity-composition model is built from solubility experiments. The parameters describing interactions between H₂O and CO₂ are independent of the absolute thermodynamic properties of the end-members and vary strongly non-linearly with pressure and temperature. The activity of water remains higher than 0.88 in CO₂-saturated solutions across the entire pressure-temperature range. In the H₂O-NaCl system, it is shown that the speciation of aqueous components can be accounted for by a thermodynamic formalism where activities are described by interaction parameters varying with intensive properties such as pressure and temperature but not with concentration or ionic strength, ensuring consistency with the Gibbs-Duhem relation. The thermodynamic model reproduces solubility experiments of halite up to 650°C and 10 kbar, and accounts for ion pairing of aqueous sodium and chloride ions with the use of associated and dissociated aqueous sodium chloride end-members whose relative proportions vary with salinity. In the H₂O-CO₂-NaCl system, an activity-composition model reproduces the salting-out effect with in-

25 teractions parameters between aqueous CO₂ and the aqueous species created by
26 halite dissolution. The proposed thermodynamic properties are compatible with
27 the THERMOCALC database (Holland and Powell, J.M.G., 2011, 29, 333-383)
28 and the equations used to retrieve the activity model in H₂O-CO₂ can be readily
29 applied to other systems, including minerals.

30 *Keywords:* Fluid-rock interactions, activity-composition model, H₂O - CO₂ -
31 NaCl, CO₂ solubility, minerals solubility, speciation, thermodynamics,
32 salting-out effect, Carbon Capture and Storage, Enhanced Oil Recovery, water
33 activity

34 1. INTRODUCTION

35 Fluids play a key role in the evolution of the lithosphere, at the surface (e.g.
36 Nesbitt and Markovics, 1997; Tipper et al., 2006), where crust is created at sub-
37 duction zones (e.g. Tatsumi, 1989; Hacker et al., 2003) as well as in the deep crust
38 and upper mantle (Newton et al., 1980; Thompson, 1992), in seawater compo-
39 sition (Edmond et al., 1979), seismicity (Chester et al., 1993), mantle dynamics
40 (Molnar et al., 1993), exhumation of subducted material (Angiboust et al., 2012),
41 ore deposits (e.g. Wilkinson and Johnston, 1996, for H₂O-CO₂-NaCl) and melting
42 (White et al., 2001). Aqueous solutions transform their host rock by dissolution
43 - precipitation reactions and ion exchange, transporting geochemical fluxes and
44 changing rock properties.

45 Concern about the environmental impacts of greenhouse gases emissions has
46 created an interest in geological carbon storage where safe, long-term storage will
47 require prediction of reactions between CO₂, aqueous formation fluids and reser-
48 voir minerals (Bickle, 2009; Wigley et al., 2012). Understanding the behavior of

49 mixed H₂O-CO₂ fluids is also important for modeling the global carbon cycle and
50 estimating metamorphic CO₂ fluxes (Kerrick and Caldeira, 1998; Becker et al.,
51 2008).

52 Description, quantitative modeling and prediction of these phenomena is based
53 on knowledge of the thermodynamic properties of end-member minerals, fluids,
54 and solutes, as well as activity-composition relationships, which describe the ther-
55 modynamic properties of mixtures as a function of their composition. Reaction
56 rates have also been shown to depend on the approach to equilibrium.

57 Although the thermodynamic properties of mineral and fluid end-members
58 are relatively well known, Oelkers et al. (2009) highlighted the importance of us-
59 ing internally consistent thermodynamic databases in geochemical modeling. Re-
60 search in metamorphic petrology has produced reliable internally consistent ther-
61 modynamic databases, amongst which the regularly updated databases of THER-
62 MOCALC (Holland and Powell, 1998; Powell et al., 1998; Holland and Powell,
63 2003, 2011) and TWEEQ (Berman, 1988; Berman and Aranovich, 1996; Ara-
64 novich and Berman, 1996) provide thermodynamics properties for more than 150
65 minerals of petrological interest each, where enthalpies of formation of various
66 end-members at standard state and their uncertainties have been estimated from
67 calorimetric measurements and phase equilibria. THERMOCALC can be used
68 with the database of Helgeson et al. (1981) for aqueous fluids and incorporates
69 the facility for error propagation and for complex activity-composition calcula-
70 tions in fluids and mineral phases. However, replication of observed fluid proper-
71 ties by activity-composition expressions, particularly for salt-rich, mixed solvent
72 fluids at pressure-temperature conditions where liquid and gas phases coexist, in
73 the regions of the critical points of CO₂ and of water, and along the critical mixing

74 line of their mixtures, has proved more challenging.

75 A number of workers has developed activity-composition relationships for flu-
76 ids that are salt-rich and/or mixed solvent and/or mixed phase or close to the criti-
77 cal point (e.g Helgeson et al., 1981; Pitzer, 1973; Pitzer and Mayorga, 1973; Pitzer
78 and Simonson, 1986; Chapman et al., 1989; Clegg and Pitzer, 1992; Clegg et al.,
79 1992; Duan and Sun, 2003; Ji et al., 2005; Duan et al., 2006; García et al., 2006;
80 Ji and Zhu, 2012). However, there is still a need for a model that:

- 81 1. replicates available data for mixed phase, salt-rich, mixed-solvent fluids
82 over a large range of pressures and temperatures;
- 83 2. allows realistic propagation of uncertainties;
- 84 3. allows dissociation of ionic solutes such as NaCl;
- 85 4. can be extended readily to more complex systems;
- 86 5. is compatible with existing thermodynamic databases and software¹.
- 87 6. is based on a relatively small number of fitted thermodynamic quantities,
88 which facilitates fits for systems where data are sparse;
- 89 7. is based on physically realistic expressions with a minimum reliance on
90 empirical expressions such as power-law series. Such an approach increases
91 the ability of a model to extrapolate beyond the limits of experimental data.

92 In this paper, we use the the Debye-Huckel ASymmetric Formalism (DH-
93 ASF) model developed by Evans and Powell (2006) to describe activity-composition

¹Mineral phases in fluid-rock systems in CO₂ sequestration and geothermal environments have a strong influence on fluid compositions via fluid-rock reaction, and almost always involve phases with complex activity-composition relationships such as ternary carbonates and feldspars. At this time, there is no software capable of combining the most recent and sophisticated activity-composition models for fluids *and* mineral phases.

94 relations between $\text{H}_2\text{O}-\text{CO}_2-\text{NaCl}$ in mixed solvent fluids up to 10 kbars and
95 650°C . The model is compatible with the computer program THERMOCALC.
96 First, phase diagrams are constructed with the ASF model applied to the binary
97 mixture of water and carbon dioxide. Then the DH-ASF model is parameterized
98 to reproduce experimental results of halite solubility in water, taking the pairing
99 of aqueous Na^+ and Cl^- into account. Finally, the effect of aqueous NaCl on
100 CO_2 solubility is fitted in the $\text{H}_2\text{O}-\text{CO}_2-\text{NaCl}$ system. The choice of the $\text{H}_2\text{O}-$
101 CO_2-NaCl chemical system is dictated by its geological importance and the large
102 number of experimental results available. The approach is designed to be readily
103 extended to additional end-members.

104 **2. APPROACH FOR THERMODYNAMIC MODELING**

105 There are a number of published approaches to modeling water-gas-minerals
106 interactions and the dissolved species they involve. The fundamental challenges
107 in modeling the thermodynamics of fluids are the choices of components and the
108 parameterizations used to describe activity-composition relationships.

109 *2.1. Terminology*

110 In the following, we use end-members for components, defined as the smallest
111 set of chemical formulae needed to describe the composition of all the phases in
112 the system (Anderson and Crerar, 1993; Spear, 1993). We model thermodynamic
113 equilibrium and the phases considered here are assumed to be chemically and
114 physically homogeneous substances bounded by distinct interfaces with adjacent
115 phases and may be minerals exhibiting solid-solutions, melts, aqueous liquids,
116 gases or supercritical fluids.

117 A key to all symbols is provided in Table 1.

118 2.2. *Thermodynamic background*

119 The Debye-Hückel limiting law (Debye and Hückel, 1923a,b) and its exten-
120 sions (e.g. Helgeson et al., 1981) have been extensively used to calculate the ther-
121 modynamic properties of solutions for geological applications but are restricted
122 to ionic strengths below 0.1 molal, whereas solutions of interest such as sedimen-
123 tary brines and metamorphic fluids have often higher ionic strengths (e.g. Houston
124 et al., 2011).

125 The Pitzer model (Pitzer, 1973; Pitzer and Mayorga, 1973; Pitzer and Simon-
126 son, 1986; Clegg and Pitzer, 1992; Clegg et al., 1992) has provided a framework
127 to express the activity coefficient, γ , of aqueous species at higher ionic strengths
128 and can be applied to salt-bearing solutions from infinite dilution to fused salt
129 mixtures. The large range of concentrations is accounted for by an activity model
130 describing a short-range force term for highly-concentrated solutions, with inter-
131 action parameters fitted to a convenient expression such as a Margules expansion
132 (e.g., Pitzer and Simonson, 1986), to which is added a Debye-Hückel term result-
133 ing from long-range ionic forces which dominate at low concentrations.

134 A different approach has been suggested by Duan et al. (2006) who proposed
135 an activity model to calculate the solubility of CO_2 in aqueous fluids by mapping
136 variations of the fugacity coefficient ϕ_{CO_2} in the two-phase mixture. ϕ_{CO_2} is linked
137 to the activity of CO_2 in the mixture, a_{CO_2} , such as $a_{\text{CO}_2} = \frac{\phi_{\text{CO}_2}}{\phi_{\text{CO}_2}^0} X_{\text{CO}_2}$, where $\phi_{\text{CO}_2}^0$
138 is the fugacity coefficient of CO_2 in its pure phase and X_{CO_2} the mole fraction
139 of CO_2 in the gas phase (Flowers, 1979). The ratio $\frac{\phi_{\text{CO}_2}}{\phi_{\text{CO}_2}^0}$ is the activity coefficient
140 γ_{CO_2} (e.g., Holland and Powell, 2003). Duan and Sun (2003) note that ϕ_{CO_2} differs
141 very little from $\phi_{\text{CO}_2}^0$ at temperatures between 0 and 260°C for all pressures lower
142 than 2kbar, and subsequently assume them to be equal so that $\gamma_{\text{CO}_2} = 1$ and

143 $a_{\text{CO}_2} = X_{\text{CO}_2}$. Duan et al. (2006) have extended this assumption to a mixing
144 scheme where ϕ_{CO_2} is only a function of pressure and temperature. However it
145 is incorrect at conditions close to the closure of the H₂O-CO₂ solvus because
146 experimental results imply $\gamma_{\text{CO}_2} \neq 1$ (e.g. Todheide and Franck, 1963). We show
147 below that $\gamma_{\text{CO}_2} = 1.07$ at 100°C - 1bar and $\gamma_{\text{CO}_2} = 1.35$ at 260°C - 2kbar.

148 Furthermore, assumptions in Duan and Sun (2003) reduce the chemical po-
149 tential of CO₂ in the gas phase ($\mu_{\text{CO}_2}^v$) to $\mu_{\text{CO}_2}^v(P, T, y) = RT \ln(P - P_{\text{H}_2\text{O}}) +$
150 $RT \ln(\phi_{\text{CO}_2}^0)$, where y is amount of CO₂ in the gas phase, T is temperature, P is
151 pressure, and $P_{\text{H}_2\text{O}}$ is boiling pressure for pure water at T . This assumes that CO₂
152 has no enthalpy of formation and describes $\mu_{\text{CO}_2}^v$ as independent of the composi-
153 tion of the mixture but sensitive to $P_{\text{H}_2\text{O}}$, even when the composition tends towards
154 pure CO₂. This model is therefore inconsistent with other work (e.g., Holland and
155 Powell, 1998), and also has the disadvantage that little information is provided on
156 the activity of water in the mixture.

157 SAFT (Statistical Associating Fluid Theory, Chapman et al., 1989) equations
158 of state (EOS) can be altered to describe variations of ϕ_{CO_2} and have been shown
159 by Ji et al. (2005) and Ji and Zhu (2012) to reproduce well the experimentally-
160 derived solubility and density of H₂O-CO₂ mixtures to which their short-range
161 parameters are fitted over the range 20-200°C and 1-600 bars. However their
162 predictive power is not greater than other semi-empirical, simpler models.

163 2.3. The ASF and DH-ASF models

164 In this study, we use both the ASF model developed by Holland and Powell
165 (2003) and its extension for aqueous species (DH-ASF, from Evans and Powell,
166 2006). ASF and DH-ASF are frameworks for activity-composition models used
167 in the THERMOCALC software together with its internally consistent database.

168 2.3.1. ASF

169 For a binary mixture, the ASF model is essentially equivalent to the sub-
 170 regular model (e.g. Thompson, 1967) where the shape of the Gibbs free energy
 171 function along the mixture is a function of two Margules parameters determining
 172 the activity coefficients needed to describe the non-ideal mixing (see De Capitani
 173 and Peters, 1982). ASF differs from the sub-regular model in that it links the shape
 174 of the Gibbs free energy function along a mixture to the relative molar volumes
 175 of the end-members, in a mixing scheme derived from the van Laar equation, and
 176 there are no ternary interaction parameters in ASF.

177 The chemical potential of an end-member l in a solution can be expressed as:

$$\mu_l(x_l) = \mu_l^0 + RT \log(x_l) + RT \log(\gamma_l) \quad (1)$$

178 where R is the ideal gas constant, T is temperature, μ_l is the chemical potential
 179 of l , μ_l^0 the chemical potential of l at standard pressure and temperature, x_l is the
 180 mole fraction of l and γ_l the activity coefficient of l . With the ASF formalism
 181 of Holland and Powell (2003), a single activity-composition model constrains the
 182 activities of the two end-members in the two phases along a binary mixture. The
 183 activity coefficient γ of l in a system with n end-members is expressed as:

$$RT \log(\gamma_l) = - \sum_{i=1}^{n-1} \sum_{j>i}^n q_i q_j W_{ij}^* \quad (2)$$

184 where i and j are end-members of the mixture, $q_i = 1 - \Phi_i$ when $i = l$, and
 185 $q_i = -\Phi_i$ when $i \neq l$ where Φ_i and W_{ij}^* are the size parameter-adjusted proportion
 186 and interaction energy defined respectively as:

$$\Phi_i = \frac{x_i \alpha_i}{\sum_{j=1}^n x_j \alpha_j} \quad (3)$$

187

$$W_{ij}^* = W_{ij} \frac{2\alpha_l}{\alpha_i + \alpha_j} \quad (4)$$

188 W_{ij} describes the magnitude of the excess Gibbs free energy function in terms of
 189 the parameters α_l attributed to each end-member. This model yields the following
 190 expression for the excess Gibbs energy $\overline{G}_m^{\text{xs}}(x)$ of a mixture comprised of n end-
 191 members:

$$\overline{G}_m^{\text{xs}}(x) = \sum_l^n x_l RT \log(\gamma_l) = \sum_{i=1}^{n-1} \sum_{j>i}^n \Phi_i \Phi_j \frac{2 \sum_{l=1}^n \alpha_l x_l}{\alpha_i + \alpha_j} W_{ij} \quad (5)$$

192 The asymmetry of the excess Gibbs free energy function is controlled by the
 193 ratio of the different α values, which describe the properties of the end-members
 194 in the mixture and have been primarily related to their relative volumes in the
 195 mixture, although these parameters may be adjusted to fit experimental constraints
 196 (Holland and Powell, 2003). There are therefore $n - 1$ independent α parameters
 197 and one of them may be set to unity (Holland and Powell, 2003). In a binary $i - j$
 198 solution where $\alpha_i = \alpha_j$, the model is symmetric and the expression of $\overline{G}_m^{\text{xs}}(x)$
 199 reduces to the sub-regular symmetric model where $\overline{G}_m^{\text{xs}}(x) = W_{ij} x_i x_j$. The ASF
 200 model assumes that neither α_i nor W_{ij} vary with the composition of the solution
 201 although they may vary with pressure and temperature to satisfy the Gibbs-Duhem
 202 equation (see Spear, 1993).

203 In the case of a binary mixture with a solvus, α_i and W_{ij} can be evaluated
 204 solely from the compositions at binodal equilibrium and/or from the conditions of
 205 critical mixing, a separation of a two-phase system from a single-phase system.
 206 Details of the derivation of the parameters are given in Appendix A where the
 207 equations have been obtained in a manner similar to the derivation of De Capitani
 208 and Peters (1982) for the subregular model. It is noteworthy that in this case the

209 chemical potentials of the end-members at standard state are not required to cal-
210 culate compositions along solution binaries; it is thus possible to construct phase
211 diagrams of binary solutions from the activity model alone, which can therefore
212 be used with any database. Uncertainties on the activity-composition model may
213 then be estimated independently from the uncertainties on the thermodynamic
214 properties of the end-members.

215 2.3.2. *DH-ASF*

216 The DH-ASF model of Evans and Powell (2006) is an extension for aqueous
217 species of the ASF model. DH-ASF shares fundamental similarities with Pitzer
218 models in that it adds a short-range force term (described by ASF) to the Debye-
219 Hückel term to express the excess Gibbs energy of a mixture. DH-ASF and ASF
220 both use standard states where the considered component is in its pure phase ($x =$
221 1) and has unit activity at any pressure and temperature. For aqueous species, DH-
222 ASF includes components for which thermodynamic data are derived from dilute
223 solutions and therefore their standard state is always hypothetical. A schematic
224 representation of the variations of the chemical potential of an aqueous species
225 with concentration is shown in appendix B together with the standard state used
226 here and the usual 1M standard state. Details of the method are described by
227 Evans and Powell (2006) and the corresponding codes have been made available
228 by Evans and Powell (2007). With this method, it is possible to model mixed
229 solvent fluids because no distinction is made between constituents forming both
230 co-solvents and what would be traditionally viewed as a solute, such as CO_2 , in
231 which case the concept of solvent and solutes becomes restrictive. The method
232 uses mean ionic compounds to describe aqueous species. For charged species
233 such as A^{n+} and B^{m-} , mean ionic compounds are obtained by summing cations

234 and anions to form $m + n$ hypothetical neutral species $(A_m B_n \pm)_{1/(m+n)}$. This
235 ensures the electro-neutrality of the mixture and allows a simple description of ion
236 pairing and common ion effects. The stoichiometric factor of $1/(m + n)$ ensures
237 that the calculated number of moles of entities present in solution is correct, which
238 is important for the entropy contributions to the free energy. For example, one
239 mole of CaCl_2 dissolving into one mole of Ca^{2+} and two moles of Cl^- , with no
240 ion pairing, would produce three moles of $(\text{CaCl}_2 \pm)_{1/3}$.

241 The thermodynamic properties of mean ionic compounds are calculated from
242 the sum of the properties of their constituents and extrapolated to standard state at
243 unit mole fraction as shown in appendix B.

244 Evans and Powell (2006, 2007) proposed parameterizations using DH-ASF
245 in several binary and ternary systems, including $\text{H}_2\text{O}-\text{CO}_2-\text{NaCl}$, at temperatures
246 greater than 400°C , where mixing parameters are either constant, linear functions
247 of temperature, or proportional to the volume of water. Such simple models do
248 not express activity-composition data adequately at lower pressures and temper-
249 atures, such as in the range of the two-phase $\text{H}_2\text{O}-\text{CO}_2$ domain (Fig. 1) because
250 experimental results imply mixing parameters vary non-linearly with pressure,
251 temperature and the properties of the solvent as shown later.

252 2.4. Selected equations of state

253 For aqueous species, we use the EOS of Holland and Powell (1998), modified
254 from Holland and Powell (1990) to incorporate the density model of Anderson
255 et al. (1991). This EOS is selected as a simple tool to estimate the thermodynamic
256 properties of aqueous species at standard state over a large range of pressures and
257 temperatures. We use the EOS for water given in the 2009 revised release of the
258 International Association for the Properties of Water and Steam (IAPWS, avail-

259 able at <http://www.iapws.org>) and the Sterner and Pitzer (1994) EOS for CO₂ to
260 calculate their respective densities, volumes and fugacities. The other routines for
261 calculation of fugacities investigated during our study are not appropriate for the
262 pressure and temperature range of interest: the CORK EOS (Holland and Pow-
263 ell, 1991) have not been constrained at temperatures lower than 100°C for either
264 water or carbon dioxide, and the EOS derived by Pitzer and Sterner (1994), cur-
265 rently used in THERMOCALC, fails to reproduce the density of water accurately
266 at temperatures less than 130°C with a maximum density at about 45°C at all pres-
267 sures less than 1kb rather than at 4°C at 1 bar. We also use the equations given by
268 the IAPWS in their 1997 release to calculate the dielectric constant of water. The
269 thermodynamic properties of the end-members used in this study are taken from
270 the THERMOCALC database (Powell et al., 1998; Holland and Powell, 1998,
271 2003, 2011).

272 3. BINARY MIXTURES OF H₂O AND CO₂

273 The phase diagram controlling the solubilities of CO₂ and H₂O in the aqueous
274 and CO₂-rich phases can be modeled with two components, for which we use
275 the end-members H₂O and CO₂. Supplementary components such as carbonate
276 species in the aqueous solutions are not required to calculate solubilities.

277 3.1. Derivation and parameterization of the activity model

278 Although the H₂O-CO₂ system has been extensively studied and different pa-
279 rameterizations are available for calculating CO₂ solubility in water or brines,
280 there is currently no activity-composition model which encompasses both low
281 pressures and temperatures and high-grade metamorphic conditions. The very

282 simple model of Holland and Powell (2003) where $W_{\text{H}_2\text{O}-\text{CO}_2} = 10.5 \frac{V_{\text{CO}_2} + V_{\text{H}_2\text{O}}}{V_{\text{CO}_2} \cdot V_{\text{H}_2\text{O}}}$,
283 $\alpha_{\text{CO}_2} = V_{\text{CO}_2}$ and $\alpha_{\text{H}_2\text{O}} = V_{\text{H}_2\text{O}}$ is based on the high pressure and temperature
284 experiments by Aranovich and Newton (1999) and gives a satisfactory fit to the
285 experimental data at pressures greater than 5 kbars but deviates from other exper-
286 imental constraints at lower pressures (Fig. 1). The models developed by Spycher
287 et al. (2003); García et al. (2006); Ji et al. (2005); Ji and Zhu (2012) or Duan
288 and co-workers (Duan et al., 1992, 1995, 1996, 2000, 2003, 2006, 2008; Duan
289 and Sun, 2003; Duan and Li, 2008; Duan and Zhang, 2006; Hu et al., 2007; Li
290 and Duan, 2007; Mao and Duan, 2009) allow calculation of the solubility of CO_2
291 and densities of mixtures at various pressures and temperatures. Akinfiyev and
292 Diamond (2010) have proposed a thermodynamic model from a compilation and
293 critical analysis of experimental results in the system $\text{H}_2\text{O}-\text{CO}_2-\text{NaCl}$ reproduc-
294 ing the solubility of CO_2 and NaCl . However, their model is restricted to a small
295 pressure-temperature range (less than 100°C and 1 kbar). As shown earlier, the
296 models of Duan and Sun (2003) and Duan et al. (2006) rely on erroneous assump-
297 tions. The thermodynamic models of Duan et al. (1992); Spycher et al. (2003); Ji
298 et al. (2005) and Ji and Zhu (2012) account for the composition of the gas phase,
299 but these models are either poorly constrained at low pressures and temperatures
300 (e.g. Duan et al., 1992, is valid at conditions $> 100^\circ\text{C}-200$ bars) or restricted to
301 low temperatures ($<100^\circ\text{C}$, Spycher et al., 2003) or low pressures (<600 bars, Ji
302 et al., 2005; Ji and Zhu, 2012). None of the above models give uncertainties on
303 their calculated parameters.

304 We use the ASF formalism, with $\alpha_{\text{H}_2\text{O}}$ set to 1 and $W_{\text{H}_2\text{O}-\text{CO}_2}$ and α_{CO_2} func-
305 tions of pressure and temperature, to model the mutual solubilities of H_2O and
306 CO_2 up to temperatures of 370°C and pressures of 3500 bars. Figure 2a-c show

307 the values of $W_{\text{H}_2\text{O}-\text{CO}_2}$ and α_{CO_2} as a function of pressure and temperature calcu-
308 lated for experimental results where both the amount of CO_2 in the aqueous phase
309 and the amount of water in the CO_2 -rich phase are measured. To do this, the exper-
310 imental data gathered by Spycher et al. (2003) at temperatures lower than 110°C
311 and the results of Todheide and Franck (1963) ranging from 50°C to 350°C and
312 from 200 to 3500 bar have been used assuming binodal equilibrium. We have also
313 used the results of Sterner and Bodnar (1991) and Mather and Franck (1992) who
314 investigated the discrepancy between the measurements of Todheide and Franck
315 (1963) and that of Takenouchi and Kennedy (1964), who report a solubility of wa-
316 ter in the CO_2 -rich phase about 20% higher at 1kb and 200°C , as noted by Joyce
317 and Holloway (1993). Sterner and Bodnar (1991) and Mather and Franck (1992)
318 found agreement with Todheide and Franck (1963) and therefore, we discarded the
319 results of Takenouchi and Kennedy (1964) obtained at temperatures greater than
320 110°C . The CO_2 solubilities measured by Takenouchi and Kennedy (1964) and
321 Takenouchi and Kennedy (1965) also differ from Todheide and Franck (1963),
322 especially at pressures below 600 bars and temperatures above 200°C , whereas
323 the results of Todheide and Franck (1963) are generally higher. The results of
324 Takenouchi and Kennedy (1965) have therefore not been used to parameterize
325 the model in $\text{H}_2\text{O}-\text{CO}_2$, but their measurements in $\text{H}_2\text{O}-\text{CO}_2-\text{NaCl}$ were used as
326 described below.

327 When not given in the original publication, experimental uncertainties have
328 been estimated as $\pm 3\%$ of the measured CO_2 content in the water-rich phase
329 and $\pm 1\%$ of the measured CO_2 content in the CO_2 -rich phase, in line with the
330 commonly reported uncertainties. Although reported compositions vary, there is
331 a general agreement between Todheide and Franck (1963) and Takenouchi and

332 Kennedy (1964) on the pressure and temperature conditions of critical mixing.
333 To the previously described experimental results, we have added the measure-
334 ments of CO₂ solubility reviewed and selected by Diamond and Akinfiev (2003)
335 in the range 0-100°C and 1-1000 bars (namely: Sander, 1912; Hähnel, 1920;
336 Kritschewsky et al., 1935; ?; Wiebe and Gaddy, 1939, 1940; Bartholomé and
337 Friz, 1956; Vilcu and Gainar, 1967; Matous et al., 1969; Stewart and Munjal,
338 1970; Malinin and Saveleva, 1972; Malinin and Kurovskaya, 1975; Zawisza and
339 Malesinska, 1981; Gillespie and Wilson, 1982; Müller et al., 1988; Namiot, 1991;
340 King et al., 1992; Teng et al., 1997; Bamberger et al., 2000; Yang et al., 2000;
341 Servio and Englezos, 2001; Anderson, 2002). When these measurements do not
342 include the composition of the gas phase, it has been evaluated for each experi-
343 mental point from a version of the model with $W_{\text{H}_2\text{O-CO}_2}$ and α_{CO_2} derived from the
344 dataset without these measurements. The estimated gas composition was given a
345 very large uncertainty (100% of the water content) to ensure that the uncertainty
346 on $W_{\text{H}_2\text{O-CO}_2}$ and α_{CO_2} is effectively constrained by the measured aqueous compo-
347 sition, giving negligible weight to the estimated gas compositions.

348 As shown on figure 2, neither $W_{\text{H}_2\text{O-CO}_2}$ nor α_{CO_2} are linear functions of pres-
349 sure and temperature, and they vary rapidly close to the phase transitions of the
350 end-members. At conditions below the critical point of water, the solvus closes
351 on the composition of water. In this case the value of α_{CO_2} tends towards $+\infty$ and
352 it is not possible to use ASF at the exact conditions of boiling water. This feature
353 is nonetheless a strong constraint on the shape of the $\alpha_{\text{CO}_2} = f(P, T)$ surface
354 (Fig. 2c). The scale of the α_{CO_2} diagram on figure 2c has been chosen to exclude
355 the very high values from experimental results close to the boiling curve of water.
356 Interestingly, the quantity $W_{\text{H}_2\text{O-CO}_2}/RT$ is remarkably linear over the range of

357 pressure and temperature where CO₂ is liquid or supercritical. α_{CO_2} is similarly
 358 nearly linear with pressure and temperature at pressures greater than 500 bars.
 359 The data scatter close to the following least squares fits to linear relationships:

$$W_{\text{H}_2\text{O-CO}_2}/RT = 5.41 - 0.276P - 1.07T * 10^{-2} \quad (6)$$

$$\alpha_{\text{CO}_2} = 0.742 - 0.0974P + 3.32T * 10^{-3} \quad (7)$$

360 with correlation coefficients (r^2) of 0.97 for $W_{\text{H}_2\text{O-CO}_2}/RT$ and of 0.96 for α_{CO_2} .
 361 However, the approximate linear relationships break down at lower pressures in
 362 the vicinities of the boiling curve of water and the critical point of CO₂. To capture
 363 the precision of the experimental results, we have parameterized $W_{\text{H}_2\text{O-CO}_2}/RT$
 364 and α_{CO_2} with polynomial functions of the density of the co-solvents H₂O and
 365 CO₂. This accounts for the abrupt changes in the parameters in pressure-temperature
 366 space (Fig. 2d). $W_{\text{H}_2\text{O-CO}_2}/RT$ and α_{CO_2} have been modeled as ratios of poly-
 367 nomials of the form N_i/D_i , with:

$$N_i = 1 + k_{i,1}.a + k_{i,2}.a^2 + k_{i,3}.a^3 + k_{i,4}.a^4 + k_{i,5}.b + k_{i,6}.b^2 \\ + k_{i,7}.b^3 + k_{i,8}.b^4 + k_{i,9}.a.b + k_{i,10}.a^2.b^2 \quad (8)$$

368

$$D_i = k_{i,11} + k_{i,12}.a + k_{i,13}.a^2 + k_{i,14}.a^3 + k_{i,15}.a^4 + k_{i,16}.b \\ + k_{i,17}.b^2 + k_{i,18}.b^3 + k_{i,19}.b^4 + k_{i,20}.a.b + k_{i,21}.a^2.b^2 \quad (9)$$

369 where i represents either $W_{\text{H}_2\text{O-CO}_2}/RT$ or α_{CO_2} , a is the density of pure H₂O and
 370 b is that of CO₂. The use of ratios of polynomial equations has been chosen to
 371 accommodate trends towards infinity. Values for $k_{W_{\text{H}_2\text{O-CO}_2}/RT}$ and $k_{\alpha_{\text{CO}_2}}$ are given
 372 in tables D1 and D2 of Appendix D.

373 Simpler expressions than equations 8 and 9 would be preferable but the ap-
374 proach used here gives accurate results for both critical mixing and reciprocal
375 solubilities of CO₂ and H₂O over the whole pressure-temperature range.

376 The adjustable parameters were calibrated by minimization of the reduced χ^2_ν
377 (defined as $\chi^2_\nu = \frac{1}{\nu} \sum_{j=1}^n \frac{(v_{Mj} - v_{Cj})^2}{\sigma_j^2}$ where v_{Mj} and v_{Cj} are measured and calcu-
378 lated values for experiment j and ν the degree of freedom) using the Levenberg-
379 Marquardt algorithm (Levenberg, 1944; Marquardt, 1963). To reduce the number
380 of adjustable parameters, an F test (as defined by Bevington and Robinson, 2002)
381 has been run where parameters were successively zeroed until the quality of the
382 fit was significantly lowered.

383 The fits to the experimental results and calculated phase diagrams are illus-
384 trated in figures 3 and 4. At pressures lower than the critical point of water, the
385 solvus closes on the boiling curve of water with a CO₂-free composition (i.e. on
386 the y axis of Fig. 3a, 3b and 3c). At pressures higher than the critical point of wa-
387 ter, the temperature of critical mixing decreases with increasing pressure (Fig. 1
388 and 3d). CO₂ solubility is also well calculated at low pressures and temperatures,
389 where the sharp difference of increase in CO₂ solubility with pressure along the
390 boiling curve of CO₂ is well reproduced (figure 4).

391 Uncertainties on the adjustable parameters of equations 8 to 9 have been es-
392 timated with the help of a Monte-Carlo simulation. The system was calculated
393 1000 times by allowing the compositions of the experimental results used to cal-
394 culate $W_{\text{H}_2\text{O-CO}_2}$ and α_{CO_2} to vary within the limits of their uncertainty (or defined
395 by the misfit of the model to the data when this was greater than experimental
396 uncertainty). The resulting covariance matrices are given in tables D1 and D2 of
397 appendix D and allow the uncertainty on the compositions to be recovered from

398 the uncertainty on $\overline{G}_m^{xs}(x)$ with the usual error propagation equation (e.g. Beving-
399 ton and Robinson, 2002, their equation 3.13).

400 The calculated parameters are strongly correlated due to the nature of the func-
401 tions and the covariance terms can consequently not be neglected.

402 An indicative map of uncertainties in calculated CO₂ solubility is provided
403 in figure 5. At pressures greater than 500 bars, experiments are generally repro-
404 duced within their uncertainties (of the order of 10% of the measured value at
405 low temperatures). At low pressure and high temperature, the model can diverge
406 from experimental values, especially in the vicinity of the boiling curve of water
407 where CO₂ solubility is very small. Below the critical point of CO₂, the model
408 reproduces the experiments less well at very low pressures where the CO₂ con-
409 centrations are very small.

410 3.2. Activities of water and carbon dioxide in saturated mixtures

411 Phase assemblages may be very sensitive to variations of the activity of water,
412 in both low- and high-grade metamorphic rocks (Greenwood, 1967; Ferry, 1984;
413 Nicollet and Goncalves, 2005; Le Bayon et al., 2006; Vidal and Dubacq, 2009).
414 The dilution of water by addition of CO₂ in solution decreases the activity of water
415 (e.g., Santosh and Omori, 2008) and may consequently decrease the temperatures
416 of dehydration reactions.

417 Figure 6 illustrates the calculated activity of water ($a_{\text{H}_2\text{O}}$, Fig. 6a) and ac-
418 tivity coefficient of water ($\gamma_{\text{H}_2\text{O}}$, Fig. 6b) in a CO₂-saturated aqueous phase in
419 the pressure-temperature range where two phases coexist. At low pressure, $a_{\text{H}_2\text{O}}$
420 decreases with increasing pressure roughly parallel to the water vapor curve. At
421 pressures higher than 1kb, $a_{\text{H}_2\text{O}}$ is more sensitive to temperature. $a_{\text{H}_2\text{O}}$ remains
422 elevated even in the vicinity of the critical curve (dashed line on Fig. 6), because

423 the composition of the mixture tends to that of water along the boiling curve of
424 water; at pressures higher than the critical point of water, the positive deviation
425 from ideal gas behavior ($\gamma_{\text{H}_2\text{O}}$ and $W_{\text{H}_2\text{O}-\text{CO}_2} > 0$) increases $a_{\text{H}_2\text{O}}$ and compensates
426 for the dilution of water by CO_2 : for example, at 270°C and 1 kbar, the water-rich
427 phase is a mixture of 18 mol. % of CO_2 and 82 mol. % of water but the water
428 activity is as high as 0.91.

429 Figure 6c and d present a_{CO_2} and γ_{CO_2} in the water-saturated CO_2 -rich phase as
430 a function of pressure and temperature. γ_{CO_2} is significantly greater than one over
431 a large range of pressures and temperatures, especially close to the boiling curve of
432 water. At 1 bar, $\gamma_{\text{CO}_2} = 1.01$ at 50°C and $\gamma_{\text{CO}_2} = 1.07$ close to 100°C . Generally,
433 the calculated a_{CO_2} decreases with temperature but increases with pressure. Very
434 low a_{CO_2} is obtained at low pressure in the vicinity of the boiling curve of water,
435 and a_{CO_2} becomes gradually less sensitive to pressure with increasing pressure.

436 3.3. Density calculations for $\text{H}_2\text{O}-\text{CO}_2$ mixtures

437 Densities calculated with the present model show a good accuracy at condi-
438 tions greater than the boiling curves of CO_2 and water, at both low and high CO_2
439 concentrations. As shown in table 3, the densities of the water phase saturated
440 in CO_2 measured by Teng et al. (1997) at temperatures lower than 20°C are re-
441 produced within 4‰ at pressures greater than 150bars. The measurements of
442 Hnedkovský et al. (1996), carried out below CO_2 saturation ($\sim 0.15\text{mol/kgH}_2\text{O}$),
443 are reproduced well away from the boiling curve of water but there is a significant
444 deviation with the calculated values ($> 10\%$) at low water density. In the gaseous
445 field of CO_2 , density calculations do not give satisfactory results either. This is
446 attributed to the use of H_2O and CO_2 as end-members in the calculations. In the
447 gaseous field of CO_2 , the volume of the CO_2 end-member is very sensitive to

448 pressure with the result that the calculated density shows a comparable sensitivity.
 449 Consequently, even if errors on the activity model are small, errors on the calcu-
 450 lated densities are large at very low densities. Similarly, the experimental results
 451 at 59°C of Li et al. (2004) are well reproduced above 100 bars after recalibration
 452 for systematic deviations (see Duan et al., 2008). A map of densities calculated
 453 over the range 0.1-3kb and 50-370°C is presented in figure 7.

454 4. ACTIVITY MODEL IN H₂O-NaCl

455 The H₂O-NaCl system has been extensively studied for decades (see Driesner
 456 and Heinrich, 2007, for a review). The solubility of halite is known to be more
 457 sensitive to temperature than to pressure (e.g. Bodnar, 1994), and NaCl dissociates
 458 into several species in solution (see Oelkers and Helgeson, 1993b; Sharygin et al.,
 459 2002) because of the pairing of Na⁺ and Cl⁻ ions. The neutral aqueous sodium
 460 chloride species NaCl⁰ is thought to dominate the associated NaCl species in solu-
 461 tion over a large range of pressure, temperature and composition (Sharygin et al.,
 462 2002), but it has been proposed that polynuclear species (Na₂Cl⁺, NaCl₂⁻, etc)
 463 also occur (e.g. Oelkers and Helgeson, 1993a,b; Sherman and Collings, 2002).
 464 The derivation of thermodynamic properties of such polynuclear species is be-
 465 yond the scope of this study and all associated species are here considered as
 466 NaCl⁰.

467 4.1. DH-ASF formalism and the Anderson et al. density model

468 With the DH-ASF model, Na⁺ and Cl⁻ ions are represented by a mean ionic
 469 end-member (NaCl[±])_{1/2} as defined in section 2.3, and the reaction describing
 470 halite NaCl_(cr) dissolution is:



471 The pairing of Na^+ and Cl^- into NaCl^0 (or its dissociation) is calculated with the
 472 reaction:



473 The total number of moles of dissolved NaCl is thus equal to $(1/2)(\text{NaCl}\pm)_{1/2} +$
 474 NaCl^0 . The subscript 1/2 will be dropped from this point onwards for convenience.
 475

476 The thermodynamic properties of $\text{NaCl}\pm$ have been calculated from that of
 477 Na^+ and Cl^- from Helgeson et al. (1981) as used in the THERMOCALC database
 478 (Holland and Powell, 2011). It has been found necessary to recalculate the heat
 479 capacity terms (Cp^0 and b_{Cp} , see Holland and Powell, 1998) of $\text{NaCl}\pm$ by fitting
 480 them to the measurements reported in Pitzer et al. (1984) as shown in figure 8a.
 481 The regressed values are $Cp^0 = -0.0417156 \text{ kJ/K}$ and $b_{Cp} = -20.8763 * 10^5$
 482 kJ.K^2 . The volumes calculated at infinite dilution of $\text{NaCl}\pm$ using the calculated
 483 heat capacity via the modified Anderson et al. (1991) density model EOS fit the
 484 volumes inferred from experimental results (Fig. 8b). However, volumes obtained
 485 above the critical temperature of water show an unreasonable pressure dependency
 486 at pressures lower than about 1 kbar, as illustrated in figure 8c. This has been
 487 identified as originating from the use of the ratio $\rho_{\text{H}_2\text{O}}/\rho_{\text{H}_2\text{O}}^0$ in the derivation of the
 488 chemical potential of Anderson et al. (1991, Fig. 8d), where $\rho_{\text{H}_2\text{O}}^0$ is the density of
 489 water at standard pressure and temperature and $\rho_{\text{H}_2\text{O}}$ is the density of water at the
 490 considered pressure-temperature. It is therefore not possible to calculate accurate
 491 densities for aqueous fluids in the range of approximately 370-550°C at pressures
 492 below about 1 kbar with this EOS, which nevertheless shows good accuracy in
 493 many geologically relevant thermal gradients.

494 The thermodynamic properties of the end-member NaCl^0 were based on those

495 of molten halite (Evans and Powell, 2006).

496 The uncertainties on the formation enthalpy ΔH_f^0 , as reported by Holland and
 497 Powell (2011) for halite, $\text{NaCl}\pm$ and NaCl^0 , are of similar relative magnitude at
 498 $\sim 0.5\%$ of their ΔH_f^0 . This corresponds to a precision of $\sim \pm 0.1$ molal for the
 499 calculation of the solubility of halite at STP.

500 4.2. Parameterization of the activity model

501 The relative amounts of $\text{NaCl}\pm$ and NaCl^0 vary non-linearly as a function of
 502 the concentration of aqueous sodium chloride and may be described by five pa-
 503 rameters between the end-members in equations 10 and 11: $W_{\text{NaCl}\pm\text{-H}_2\text{O}}$, $W_{\text{NaCl}^0\text{-H}_2\text{O}}$,
 504 $W_{\text{NaCl}\pm\text{-NaCl}^0}$, $\alpha_{\text{NaCl}\pm}$ and α_{NaCl^0} . It is assumed that $W_{\text{NaCl}\pm\text{-NaCl}^0} = 0$ as this term
 505 has little effect on the calculated equilibria.

506 Solubility, density and conductivity measurements were used to parameterize
 507 the activity model. Selected solubility experiments range from 15 to 650°C and
 508 from 1 bar to 10 kbar (table 2). The data are mostly consistent, with the exception
 509 of the high pressure measurements of Sawamura et al. (2007) who report solubility
 510 values for halite higher by up to 2% than the measured values at 2-3kb and 25°C
 511 of Adams (1931, figure 9).

512 Measurements of the conductance of NaCl solutions are used to estimate the
 513 degree of dissociation of NaCl^0 into Na^+ and Cl^- (eq. 11) via:

$$x_{\text{NaCl}\pm} = \Lambda\epsilon/\Lambda e \quad (12)$$

514 where $x_{\text{NaCl}\pm}$ is the fraction of NaCl dissolved as $\text{NaCl}\pm$, $\Lambda\epsilon$ is the experimen-
 515 tally determined equivalent conductance and Λe is the equivalent conductance
 516 of a hypothetical completely dissociated NaCl solution of the same effective ionic
 517 strength (Oelkers and Helgeson, 1988). The procedure selected to calculate $\Lambda\epsilon/\Lambda e$

518 is described in Appendix C, and we used the measurements of Bianchi et al.
519 (1989), Chambers et al. (1956) and Quist and Marshall (1968). At 25°C and 1
520 bar, the calculated $\Lambda\epsilon/\Lambda e$ indicate that, within uncertainties of the data, correc-
521 tions and equations used, at least 95% of the aqueous NaCl is dissociated up to
522 5.35 molal, in agreement with Monica et al. (1984) but strikingly different from
523 the results of Sherman and Collings (2002) whose molecular dynamic simulations
524 predict about 50% of aqueous NaCl to be as NaCl^0 or larger polynuclear species
525 at 6 molal. Only values of $x_{\text{NaCl}\pm}$ estimated from conductance measurements have
526 been used in this work. At constant molality, $\Lambda\epsilon/\Lambda e$ decreases with temperature
527 and increases with pressure, as noted by Oelkers and Helgeson (1988) and shown
528 in figure 10.

529 The calculated volume of the $\text{NaCl}\pm$ end-member at its hypothetical pure stan-
530 dard state depends on both 1) the thermodynamic properties of the usual hypothet-
531 ical Na^+ and Cl^- 1 molal aqueous species derived from infinite dilution and 2) on
532 the interaction parameters $W_{\text{NaCl}\pm\text{-H}_2\text{O}}$ and $\alpha_{\text{NaCl}\pm}$ because they affect the chemical
533 potential of the $\text{NaCl}\pm$ end-member within the DH-ASF framework. NaCl being
534 largely dissociated under 100°C, NaCl^0 has little effect on the Gibbs energy of
535 the mixture and on its pressure dependency. Consequently, the pressure depen-
536 dency of $W_{\text{NaCl}\pm\text{-H}_2\text{O}}$ and $\alpha_{\text{NaCl}\pm}$ are constrained mainly by the chosen density
537 measurements (Surdo et al., 1982). The temperature dependency of these param-
538 eters has been estimated together with that of $W_{\text{NaCl}^0\text{-H}_2\text{O}}$ and $\alpha_{\text{NaCl}\pm}$ by fitting
539 high-temperature solubility experiments (Fig. 9a) and the calculated degree of
540 association (Fig. 10a, equation C1).

541 The following expressions have been found to provide a good description of
542 the system in the pressure-temperature range 1bar-10kbar and 20-650°C, as shown

543 in figures 9, 10 and 11:

$$W_{\text{NaCl}^0\text{-H}_2\text{O}} = C_1 + C_2 \cdot P + C_3 \cdot T + C_4 \cdot P^2 \quad (13)$$

$$\alpha_{\text{NaCl}^0} = C_5 + C_6 \cdot P + C_7 \cdot T \quad (14)$$

544

$$W_{\text{NaCl}\pm\text{-H}_2\text{O}} = C_8 + C_9 \cdot T_{400} + C_{10} \cdot T_{400}^2 + C_{11} \cdot P + C_{12} \cdot P^2 \quad (15)$$

$$\alpha_{\text{NaCl}\pm} = C_{13} + C_{14} \cdot T + (C_{15} + C_{16} \cdot T)P \quad (16)$$

545 where T_{400} is temperature below 400K such as $W_{\text{NaCl}\pm\text{-H}_2\text{O}}$ is independent of tem-
 546 perature above 400K. Values for the C constants are given in Table D3 of Ap-
 547 pendix D.

548 4.3. Results and error propagation

549 The correlation between the calculated and measured solubilities is good (Fig.
 550 9). This model gives a better fit to high-temperatures data than the model of Mao
 551 and Duan (2008, dotted line on Fig. 9). The obtained parameters agree well with
 552 the results of Aranovich and Newton (1996) who found that the system is very
 553 close to ideality around 2 kbar and 500°C ($W_{\text{NaCl}^0\text{-H}_2\text{O}} = 0.56 \text{ kJ}\cdot\text{mol}^{-1}$). Density
 554 measurements in the aqueous phase are very well reproduced below the critical
 555 point of water and are in close agreement with the model of Driesner (2007). At
 556 higher temperatures, our model diverts from the model of Driesner (2007) (Fig.
 557 11b and c) for pressures around 1 kbar and below. The calculated dissociation of
 558 NaCl^0 presented in figure 10a is consistent with the measurements of Quist and
 559 Marshall (1968) as they show the same variations with pressure and temperature
 560 but appear offset from a few to about 15 percents, which could not be reproduced
 561 without allowing unrealistically low values for α_{NaCl^0} . The uncertainties associ-
 562 ated with the original values of $\Lambda\epsilon$ and Λ_0 reported by Quist and Marshall (1968)

563 cumulate to a minimal uncertainty of about 10% of the given $x_{\text{NaCl}\pm}$ value at water
564 densities below 0.5 and between 4 and 10% at higher densities. Because 1) uncer-
565 tainties associated with the use of equations C2 and C3 are unknown, 2) the pos-
566 sible role of large polynuclear species, although unclear (Sharygin et al., 2002),
567 can not be ruled out and 3) the low ratio of $\text{NaCl}\pm$ to NaCl^0 makes $W_{\text{NaCl}\pm-\text{H}_2\text{O}}$
568 poorly constrained at temperatures greater than 500°C, we have adopted the sim-
569 plest expression that could be derived for the activity model in which $W_{\text{NaCl}\pm-\text{H}_2\text{O}}$
570 is independent of temperature above 400K and $\alpha_{\text{NaCl}\pm}$ varies linearly with pres-
571 sure but with a temperature-dependent slope. Overall, the model gives a better fit
572 to the data and is in better agreement with other models for high density solutions
573 than for low density solutions, partially because of the use of the density model
574 of Anderson et al. (1991), but also because the lack of theory together with the
575 scarcity of precise high-temperature high-concentration experimental data made
576 assumptions on the pressure-temperature dependency of the thermodynamic pa-
577 rameters necessary.

578 Error propagation has been performed by a Monte-Carlo simulation where the
579 system has been refitted 100 times, by varying the original experimental results
580 within the misfit of the model to the data and the enthalpy of formation of the
581 aqueous species within their uncertainties. To simplify the propagation of errors
582 on the activity model, the correlation of uncertainties associated with the enthalpy
583 of formation of the aqueous species given in the THERMOCALC database has
584 been neglected. The covariance matrix associated with C_1 to C_{16} is given in Table
585 D3.

586 **5. THE H₂O-CO₂-NaCl SYSTEM**

587 The solubility of CO₂ in the water phase decreases with increasing salinity
588 of the aqueous phase (termed salting-out, e.g.: Markham and Kobe, 1941; Drum-
589 mond, 1981; Nighswander et al., 1989; Rumpf et al., 1994). The combination
590 of the subsystems H₂O-CO₂ and H₂O-NaCl needs two additional interaction pa-
591 rameters to describe H₂O-CO₂-NaCl: $W_{\text{CO}_2\text{-NaCl}^0}$ and $W_{\text{CO}_2\text{-NaCl}\pm}$. Salting-out
592 implies positive values for these parameters. The magnitudes of $W_{\text{CO}_2\text{-NaCl}^0}$ and
593 $W_{\text{CO}_2\text{-NaCl}\pm}$ are expected to be high given that NaCl is barely incorporated in the
594 CO₂-rich phase in the absence of water, even at high pressure and temperature: the
595 measurements of Zakirov et al. (2007) indicate a NaCl mole fraction of 30×10^{-7}
596 in the CO₂ phase at 670 bars and 400°C. In H₂O-CO₂-NaCl, taking the CO₂-rich
597 phase to be free of NaCl is an acceptable approximation up to at least 300°C (e.g.
598 Hu et al., 2007, and references herein). With this assumption, the solubility of
599 CO₂ in the aqueous NaCl solution can be calculated by minimizing the Gibbs
600 free energy of the system, composed of a water-saturated CO₂-rich phase and of
601 the aqueous phase at fixed NaCl content. The relative proportions of NaCl⁰ and
602 NaCl[±] are calculated by solving equation 11 with the appropriate interaction pa-
603 rameters (eq. 8,9,13,14,15,16).

604 As pointed out by Hu et al. (2007), there is currently no accurate model to
605 predict the solubility of CO₂ in NaCl brines at temperatures greater than about
606 60°C, mainly due to the scarcity of experimental results at these pressures and
607 temperatures. In particular, the measurements of Takenouchi and Kennedy (1965)
608 (ranging up to 1400 bars and 450°C) are not in agreement with other experiments
609 at pressures below 300 bars, some of which we used here (Ellis and Golding,
610 1963; Drummond, 1981; Nighswander et al., 1989; Rumpf et al., 1994; Kiepe

611 et al., 2002). The measurements of Takenouchi and Kennedy (1965) at zero NaCl
 612 content are also inconsistent (by up to 15%, see Fig. 12b) with the measurements
 613 of Todheide and Franck (1963) which we used to constrain the H₂O-CO₂ activity
 614 model. However, all the data of Takenouchi and Kennedy (1965) at $x_{NaCl} > 0$
 615 have been kept in our regression as they are the major source of measurements
 616 available above 500 bars.

617 It was assumed that $W_{CO_2-NaCl^0} = W_{CO_2-NaCl\pm}$ because the quality of the fit to
 618 the data is not statistically sensitive to the ratio $W_{CO_2-NaCl^0}/W_{CO_2-NaCl\pm}$. $W_{CO_2-NaCl^0}$
 619 and $W_{CO_2-NaCl\pm}$ may then be estimated from solubility experiments independently
 620 of the thermodynamic properties of pure H₂O and CO₂ and of their uncertain-
 621 ties. However the values depend on the activity models in H₂O-CO₂ and H₂O-
 622 NaCl. As observed in the H₂O-CO₂ system, the quantity $W_{CO_2-NaCl\pm}/(RT)$ shows
 623 smoother variations in pressure-temperature space than $W_{CO_2-NaCl\pm}$, although both
 624 values increase strongly with pressure especially under 100 bars. For this reason,
 625 $W_{CO_2-NaCl\pm}$ has been parameterized as a function of the natural logarithm of pres-
 626 sure:

$$W_{CO_2-NaCl\pm}/(RT) = D_1 + D_2 \ln P + D_3 T + D_4 T \ln P + D_5 (\ln P)^2 \quad (17)$$

627 where pressure is in bar and temperature in Kelvin. Values for D_1 to D_5 are given
 628 in table D4.

629 Figure 12 illustrates the calculated salting-out effect and presents the quality
 630 of the fit of the model to some of the experimental data. Error propagation has
 631 been carried out as in the previous systems by a Monte-Carlo simulation where
 632 experimental uncertainties are estimated from the misfit of the model with the ex-
 633 perimental results. The covariance matrix for D_1 to D_5 is given together with their
 634 values in table D4. The correlation of uncertainties between parameters regressed

635 for the activity models in the subsystems $\text{H}_2\text{O}-\text{CO}_2$ and $\text{H}_2\text{O}-\text{NaCl}$ and this sys-
636 tem has been neglected because uncertainties from experiments and the models in
637 the subsystems are smaller than in $\text{H}_2\text{O}-\text{CO}_2-\text{NaCl}$.

638 **6. DISCUSSION**

639 *6.1. Accuracy and advantages of the method*

640 The method used here to parameterize the $\text{H}_2\text{O}-\text{CO}_2$ activity model is inde-
641 pendent of the thermodynamic properties of the co-solvents and successfully re-
642 produces the experimentally-derived phase diagram over the whole two-phase do-
643 main. The solubility of CO_2 is also calculated well by other models, in particular
644 Duan et al. (2006, figure 3), although it has been shown that this model does not
645 provide a correct derivation of the chemical potential of CO_2 . The models of
646 Spycher et al. (2003) and Akinfiyev and Diamond (2010) give excellent fits to the
647 aqueous phase experimental results at temperatures below 100°C . The principal
648 advantages of the model presented here are 1) the facility to model the CO_2 -rich
649 phase, 2) the wider pressure-temperature range of applicability, and 3) the ease
650 of error propagation provided by separate uncertainties for the activity model and
651 the end-members.

652 In the $\text{H}_2\text{O}-\text{NaCl}$ system, the DH-ASF activity model reproduces the experi-
653 mental data on the solubility of halite over a wide range of pressures and temper-
654 atures. Here, the form of the pressure and temperature dependency of the activity
655 parameters have been fitted to solubilities, densities and conductivity measure-
656 ments, giving reasonable values for $\alpha_{\text{NaCl}\pm}$ and α_{NaCl^0} whose variations over 10
657 kb and 600°C do not exceed 0.4 and 0.8 α unit, respectively. Their pressure
658 derivatives, implied by density measurements, are particularly small (at a max-

imum magnitude of $5.10^{-3} \text{ kbar}^{-1}$) and of opposite signs, making it difficult to link them to variations of the properties of the solvent. The pressure dependencies of $W_{\text{NaCl}^0\text{-H}_2\text{O}}$ and $W_{\text{NaCl}\pm\text{-H}_2\text{O}}$ are similarly small, which is imposed by the insensitivity of halite solubility to pressure.

Results in $\text{H}_2\text{O} - \text{CO}_2 - \text{NaCl}$ are compared in figure 12 to the model of Duan and Sun (2003) on which the model of Duan and Zhang (2006) is based. At pressures and temperatures under 100°C and 100 bars, our model gives results very similar to Duan and Sun (2003). At higher pressures and temperatures, the model of Duan and Sun (2003) gives a better fit to the data of Takenouchi and Kennedy (1965), which are often lower than expected from the measurements of Todheide and Franck (1963), well reproduced by our model. For this reason, our model gives solubilities greater than the data of Takenouchi and Kennedy (1965) and the model of Duan and Sun (2003) at pressures and temperatures where Todheide and Franck (1963) and Takenouchi and Kennedy (1965) are not in agreement (Fig. 12). However, the curvature of the CO_2 solubility is quite similar for both models at NaCl concentrations below 3 molal. The model presented in this study has been fitted with essentially the same dataset as in Duan and Sun (2003) for the system $\text{H}_2\text{O} - \text{CO}_2 - \text{NaCl}$, where high-pressure-temperature measurements are restricted below about 4 molal NaCl. However our model gives different extrapolation to higher concentrations than Duan and Sun (2003, e.g. Fig. 12b), where their approach predicts an increase of the CO_2 solubility with increasing NaCl molality, which might happen if for instance the formation of Na carbonate complexes increases the solubility of CO_2 , but is not supported by any data to our knowledge. Our model, whose parameters do not depend on concentration, predicts a continuous decrease in CO_2 solubility with increasing salinity over the

684 entire pressure-temperature range and up to 10 molal NaCl.

685 6.2. Range of applicability and limitations

686 The pressure-temperature range of the activity model proposed for H₂O-CO₂
687 is limited to the two-phase domain. Equations A11, A13, A18 and A19 pro-
688 vide a simple and accurate parameterization of the system H₂O-CO₂ but only
689 over pressure-temperature conditions where two phases coexist. The parameter-
690 ization can not be extrapolated to the one-phase domain below the critical point
691 of water (Fig. 1): although $a_{\text{CO}_2}/\alpha_{\text{H}_2\text{O}}$ tends towards infinity near the boiling
692 curve of water, there is no simple relation between a_{CO_2} and $V_{\text{CO}_2}/V_{\text{H}_2\text{O}}$. Ex-
693 trapolation of the model towards low temperatures or high pressures in the liquid
694 field of CO₂ is speculative as there are few experimental results to constrain its
695 pressure-temperature dependency. It has been noted in section 2.2 and figure 2b
696 that away from the boiling curve of water and critical point of carbon dioxide,
697 both $W_{\text{H}_2\text{O-CO}_2}/RT$ and a_{CO_2} approximate a linear behavior. However, it is un-
698 likely that the observed trends can be extrapolated over a larger range of pressures
699 and temperatures. Models (e.g. Johnson, 1991; Holland and Powell, 2003, Fig.
700 1) suggest that the critical temperature increases significantly at pressure greater
701 than 3.5 kb, implying that $W_{\text{H}_2\text{O-CO}_2}$ increases with increasing pressure, opposite
702 to the trend observed below 3500 bars. As shown in figure 13, the departures at
703 higher temperatures from the model of Holland and Powell (2003), calibrated in
704 the one-phase domain, imply that the decrease of $W_{\text{H}_2\text{O-CO}_2}/RT$ with temperature
705 (Fig. 2) is likely to be much smaller or reversed in the one-phase domain. In the
706 two-phase domain, differences between the model of Holland and Powell (2003)
707 and this model, of the order of 1.5 kJ/mol for $W_{\text{H}_2\text{O-CO}_2}$ around 3kbar and 200°C
708 (Fig. 13), are very significant for the solvus as illustrated on figure 3d. For the

709 same conditions, the precision on the activity model in this work is that obtained
 710 from the experimental data, of the order of 0.1 kJ/mol for $W_{\text{H}_2\text{O-CO}_2}$ and 0.01 for
 711 $\alpha_{\text{CO}_2}/\alpha_{\text{H}_2\text{O}}$.

712 There are therefore abrupt changes in the parameters describing the thermo-
 713 dynamic properties of the mixture both along the critical mixing curve (Fig. 13)
 714 and along along the phase transitions of the end-members (e.g. steps in $W_{\text{H}_2\text{O-CO}_2}$
 715 along the boiling curve of CO_2 , Fig. 2d; $\alpha_{\text{CO}_2} \rightarrow \infty$ along the boiling curve of
 716 water, Fig. 2c).

717 For these reasons the model (equations 8-9) should not be extrapolated to the
 718 one-phase region (Fig. 1) where the model of Holland and Powell (2003) is ap-
 719 propriate (and conversely the model of Holland and Powell (2003) should not be
 720 used in the two-phase domain). The critical curve which delimits the domain of
 721 applicability can be closely approximated from the critical point of water up to
 722 3500 bars by:

$$T_C = q_1 + q_2 \cdot P + q_3 \cdot P^2 + q_4 \cdot \log(P) \quad (18)$$

723 where q_1 to q_4 are constants obtained by regression analysis ($R^2 = 0.993$) of
 724 the data of Todheide and Franck (1963) and Takenouchi and Kennedy (1964):
 725 $q_1 = 195.3$, $q_2 = 90.36$, $q_3 = -8.945$, $q_4 = -107.9$.

726 Another limitation of our approach (derived from the phase rule and relying
 727 on a minimum number of end-members used to describe the system) is that spe-
 728 ciation (and its effects) is hard to predict for high concentrations although easy
 729 to reproduce. In other words, experimental results are necessary to parameterize
 730 the model. For instance, the formation of Na carbonate complexes might result
 731 in increasing CO_2 solubility with increasing Na concentration, when our model
 732 predicts a continuous decrease of CO_2 solubility with increasing salinity. For the

733 same reason, CO_2 solubility in rock-buffered systems may be different from what
734 is estimated with this model.

735 7. CONCLUSIONS

736 The model presented here is unique in that it replicates available data for mixed
737 phase, salt-rich, mixed-solvent fluids close to the critical end point, allows real-
738 istic propagation of uncertainties, simulates dissociation of ionic solutes such as
739 NaCl , can be extended readily to more complex systems as it uses transferable pa-
740 rameters, is compatible with existing thermodynamic databases and software, and
741 is based, as far as possible, on physically realistic expressions with a minimum
742 reliance on empirical expressions such as power-law series. The large number of
743 empirically fitted constants is however a drawback to a well-constrained activity
744 model.

745 It is possible to calculate accurate phase diagrams for CO_2 - H_2O mixtures in
746 the two-phase domain with macroscopic interaction parameters and associated
747 uncertainties independently of the standard state chemical potentials of water and
748 carbon dioxide. Such calculations are straightforward, fast, lead to a unique result
749 and do not depend on the quality of the chosen thermodynamic database. They
750 can be implemented in Gibbs energy minimization routines (e.g. Connolly, 2009;
751 De Capitani and Petrakakis, 2010).

752 The interaction parameters $W_{\text{H}_2\text{O}-\text{CO}_2}$ and a_{CO_2} calculated from experimental
753 results show non-linear variations with pressure and temperature, reflecting sig-
754 nificant changes of solubilities and volumes for example along the vapor-liquid
755 transition curves of water and carbon dioxide. This contrasts with the description
756 of the higher temperature-pressure conditions applicable to metamorphic petrol-

757 ogy where the linear relation $W_G = W_H - T * W_S + P * W_V$ holds for the
758 many systems described by the subregular model or the ASF formalism. As a
759 consequence, it is not possible to extrapolate mixing parameters in the one-phase
760 domain from compositions at equilibrium in the two-phase domain in the H₂O-
761 CO₂ system.

762 An activity model in the H₂O-NaCl system was derived with a similar ther-
763 modynamic formalism, DH-ASF (Evans and Powell, 2006), which uses hypothet-
764 ical end-members with unit activity at standard state for aqueous species. This
765 model requires a small number of concentration-independent interaction paramet-
766 ers, which we parameterized up to 10kbars and 650°C as a function of pressure
767 and temperature using density, conductivity and solubility measurements.

768 The activity models in H₂O-CO₂ and H₂O-NaCl were combined to derive an
769 activity model in the H₂O-CO₂-NaCl system where the decrease of CO₂ solubility
770 with salinity is reproduced by positive values for W parameters between dissolved
771 NaCl and CO₂. It is shown that this approach extrapolates to high salinities with a
772 continuous decrease in CO₂ solubility, in contrast with the model of Duan and Sun
773 (2003). The fit to the experimental data is good and uncertainties on all parameters
774 of the activity model are estimated.

775 Addition of activity models for aqueous species and gases to the THERMO-
776 CALC database with the DH-ASF formalism is in progress (e.g. Evans et al.,
777 2010).

778 8. ACKNOWLEDGMENTS

779 This work was supported by the EU Marie Curie GRASP RTN and the NERC
780 through the CRIUS consortium. We thank Éric Lewin for help in regression anal-

781 ysis and Roger Powell, Tim Holland, Niko Kampman, Olivier Namur, Oli Shorttle
782 and Ed Tipper for helpful discussions. Jacques Schott (A.E.) and three anonymous
783 reviewers are thanked for their numerous comments and suggestions on previous
784 versions of the manuscript.

ACCEPTED MANUSCRIPT

785 **APPENDIX A**

786 It is demonstrated here that if unmixing occurs in a binary $i - j$ solution,
 787 it is possible to calculate the values of the parameters W_{ij} and α_i/α_j from the
 788 compositions of the coexisting phases x_1 and x_2 at equilibrium, i.e. from the
 789 binodal solvus.

790 In a binary $i - j$ solution, where x is the proportion of the j end-member so
 791 that $x_i = 1 - x$, chemical potentials can be expressed as (e.g. Guggenheim, 1977):

$$\mu_i(x) = \bar{G}_m(x) - x \frac{\delta \bar{G}_m(x)}{\delta x} \quad (\text{A1})$$

792

$$\mu_j(x) = \bar{G}_m(x) + (1 - x) \frac{\delta \bar{G}_m(x)}{\delta x} \quad (\text{A2})$$

793 where $\bar{G}_m(x)$ is the molar Gibbs free energy of the mixture:

$$\begin{aligned} \bar{G}_m(x) = (1 - x)\mu_i^0 + x\mu_j^0 + RT(1 - x) \log(1 - x) \\ + RTx \log(x) + \bar{G}_m^{\text{xs}}(x) \end{aligned} \quad (\text{A3})$$

794 The Gibbs free energy of mixing $\bar{G}_m^{\text{mix}}(x)$ is the energy added to the mechanical
 795 mixture of the pure end-members:

$$\bar{G}_m^{\text{mix}}(x) = RT(1 - x) \log(1 - x) + RTx \log(x) + \bar{G}_m^{\text{xs}}(x) \quad (\text{A4})$$

796 Expressed with the ASF formalism, $\bar{G}_m^{\text{xs}}(x)$ reduces to:

$$\bar{G}_m^{\text{xs}}(x) = \frac{2\alpha_i\alpha_j W_{ij}(1 - x)x}{(\alpha_i + \alpha_j)(\alpha_i(1 - x) + \alpha_j x)} \quad (\text{A5})$$

797 Note that in an ideal mixing scheme, $\bar{G}_m^{\text{xs}}(x) = 0$ and $\bar{G}_m^{\text{mix}}(x)$ is negative with
 798 a temperature-dependent minimum value at $x = 0.5$ reflecting the entropy of
 799 mixing.

800 Equilibrium implies that the chemical potential of each end-member must be
801 the same in each phase:

$$\mu_i(x)_{x=x_1} = \mu_i(x)_{x=x_2} \quad (\text{A6})$$

$$\mu_j(x)_{x=x_1} = \mu_j(x)_{x=x_2} \quad (\text{A7})$$

802 Using equation A1 and equation A2, we obtain the two conditions A8 and A9:

$$\frac{\delta \bar{G}_m(x_1)}{\delta x} = \frac{\delta \bar{G}_m(x_2)}{\delta x} \quad (\text{A8})$$

803 and

$$\bar{G}_m(x_1) - \bar{G}_m(x_2) = (x_1 - x_2) \frac{\delta \bar{G}_m(x_1)}{\delta x} \quad (\text{A9})$$

804 where

$$\begin{aligned} \frac{\delta \bar{G}_m(x)}{\delta x} = & \mu_j^0 - \mu_i^0 + RT \log\left(\frac{x}{1-x}\right) \\ & + \frac{2\alpha_i\alpha_j W_{ij}(\alpha_i(x-1)^2 - \alpha_j x^2)}{(\alpha_i + \alpha_j)(\alpha_i(x-1) - \alpha_j x)^2} \end{aligned} \quad (\text{A10})$$

805 In the special case of a symmetric solvus, the gradient of Gibbs energy with com-
806 position $\frac{\delta \bar{G}_m(x)}{\delta x} = 0$ at binodal compositions.

807 Combining equations A8 and A9 with equation A5 gives

$$W_{ij} = RT\left((1-x_2) \log\left(\frac{1-x_2}{1-x_1}\right) + x_2 \log\left(\frac{x_2}{x_1}\right)\right) * D \quad (\text{A11})$$

808 where D is given by:

$$D = -\frac{(\alpha_i + \alpha_j)(\alpha_i(x_1 - 1) - \alpha_j x_1)^2(\alpha_i(x_2 - 1) - \alpha_j x_2)}{2\alpha_i^2\alpha_j^2(x_1 - x_2)^2} \quad (\text{A12})$$

809 and

$$\alpha_j = \frac{\alpha_i(2(x_1 - 1)(x_2 - 1) \log\left(\frac{x_1-1}{x_2-1}\right) + (x_1 + x_2 - 2x_1x_2) \log\left(\frac{x_1}{x_2}\right))}{(-x_2 + x_1(2x_2 - 1)) \log\left(\frac{x_1-1}{x_2-1}\right) - 2x_1x_2 \log\left(\frac{x_1}{x_2}\right)} \quad (\text{A13})$$

810 Defining $\alpha_i = 1$, only one of α_i and α_j varies independently and D can be ex-
 811 pressed as $D = E/F$, where E and F depend only on x_1 and x_2 :

$$E = 2((x_1(2x_2 - 1) - x_2) \log\left(\frac{x_1 - 1}{x_2 - 1}\right) - 2x_1x_2 \log\left(\frac{x_1}{x_2}\right))^2 (2(x_1 - 1)(x_2 - 1) \log\left(\frac{x_1 - 1}{x_2 - 1}\right) + (-2x_2x_1 + x_1 + x_2) \log\left(\frac{x_1}{x_2}\right))^2 \quad (\text{A14})$$

812

$$F = (x_2 - x_1) \left((x_1 - 1) \log\left(\frac{x_1 - 1}{x_2 - 1}\right) - x_1 \log\left(\frac{x_1}{x_2}\right) \right)^2 + ((x_2 - 1) \log\left(\frac{x_1 - 1}{x_2 - 1}\right) - x_2 \log\left(\frac{x_1}{x_2}\right)) \left((-3x_2 + x_1(4x_2 - 3) + 2) \log\left(\frac{x_1 - 1}{x_2 - 1}\right) + (-4x_2x_1 + x_1 + x_2) \log\left(\frac{x_1}{x_2}\right) \right) \quad (\text{A15})$$

813 The conditions of critical mixing (consolute point along isotherms or isobars on
 814 phase diagrams such as presented in figure 3) are reached when:

$$\frac{\delta^2 \bar{G}_m(x_c)}{\delta x^2} = \frac{RT_C}{x_C - x_C^2} - \frac{4\alpha_i^2 \alpha_j^2 W_{ij}}{(\alpha_i + \alpha_j)(\alpha_i + x_C(\alpha_j - \alpha_i))^3} = 0 \quad (\text{A16})$$

815 and

$$\frac{\delta^3 \bar{G}_m(x_c)}{\delta x^3} = RT_C \left(\frac{1}{(x_C - 1)^2} - \frac{1}{x_C^2} \right) + \frac{12\alpha_i^2 \alpha_j^2 W_{ij} (\alpha_j - \alpha_i)}{(\alpha_i + \alpha_j)(\alpha_i + x_C(\alpha_j - \alpha_i))^4} = 0 \quad (\text{A17})$$

816 where T_C is the critical temperature. This defines W_{ij} as:

$$W_{ij} = RT_C \frac{(\alpha_i + \alpha_j)(\alpha_i(x_C - 1) - \alpha_j x_C)^3}{4\alpha_i^2 \alpha_j^2 (x_C^2 - x_C)} \quad (\text{A18})$$

817 and α_j as

$$\alpha_j = \frac{\alpha_i(x_C^2 - 1)}{x_C(x_C - 2)} \quad (\text{A19})$$

818 The two coexisting compositions can be calculated by minimizing the Gibbs free
 819 energy of the system (see Connolly, 2009; De Capitani and Petrakakis, 2010) or
 820 by solving equations A8 and A9 for x_1 and x_2 . Equation A8 gives:

$$\frac{2\alpha_i^2\alpha_j^2W_{ij}(x_1 - x_2)(\alpha_i(x_1 + x_2 - 2) - \alpha_j(x_1 + x_2))}{(\alpha_i + \alpha_j)(\alpha_i(x_1 - 1) + \alpha_jx_1)^2(\alpha_i(x_2 - 1) - \alpha_jx_2^2)} + RT\left(\log\left(\frac{1 - x_2}{1 - x_1}\right) + \log\left(\frac{x_1}{x_2}\right)\right) = 0 \quad (\text{A20})$$

821 Equation A9 gives:

$$\frac{-2\alpha_i^2\alpha_j^2W_{ij}(x_1 - x_2)^2}{(\alpha_i + \alpha_j)(\alpha_i(x_1 - 1) + \alpha_jx_1)^2(\alpha_i(x_2 - 1) - \alpha_jx_2^2)} + RT\left((x_2 - 1)\log\left(\frac{1 - x_2}{1 - x_1}\right) + x_2\log\left(\frac{x_1}{x_2}\right)\right) = 0 \quad (\text{A21})$$

822 **APPENDIX B**

823 The DH-ASF formalism allows description of both the Debye-Hückel effect
824 arising from long-range interactions at low concentrations and short-range forces
825 at high concentrations. The evolution of the chemical potential of the aqueous
826 species A is illustrated in figure B1. The chemical potential of A at standard
827 state μ_A^0 is defined at $x_A = 1$. μ_A^0 is augmented from the ideal line at $x = 1$
828 by the sum of all non-ideal contributions: long-range electrostatic forces at low
829 concentrations where μ is below the ideal mixing line and short-range interactions
830 at higher concentrations. At high dilutions of A , μ_A approaches ideal solution
831 (dashed line on Fig. B1). With increased concentration of A , μ_A evolves to $\mu_A <$
832 μ_{ideal} (e.g. at $x = x_1$) due to the Debye-Hückel effect. The effect of long-
833 range interactions has been limited in the modeling to a maximum of 0.1 molal
834 by Evans and Powell (2006). For solutions more concentrated than 0.1 molal,
835 the activities of the end-members in solution are described by the short-range
836 interaction parameters of the ASF model. On figure B1, these constrain the part
837 of the diagram where μ_A is greater than the line of ideal mixing (e.g. at $x = x_2$).

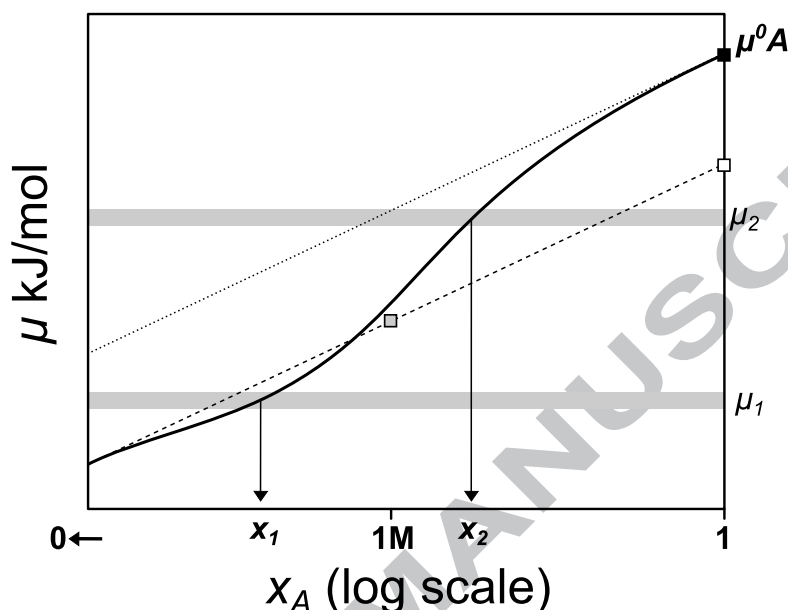


Figure B1: Schematic illustration of the relationship between chemical potential of the aqueous species A and its concentration x_A in the DH-ASF formalism. The solid line indicates the measured chemical potential. The broken line shows the chemical potential of an ideal solution referenced to infinite dilution for A . The usual 1M standard state is indicated with a gray square, and its equivalent projected at $x=1$ along the ideal mixing line shown with an open square. The dotted line shows the chemical potential for an ideal solution referenced to a hypothetical ideal solution at $x = 1$. μ_A^0 , the standard state chemical potential of A used in the DH-ASF formalism, is shown with a closed square at $x_A = 1$, it differs from the ideal mixing line by the sum of long- and short-range interactions to the excess free energy. Modified after Evans and Powell (2006).

838 **APPENDIX C**

839 Measurements of the conductance of NaCl solutions are used to estimate the
840 degree of dissociation of NaCl⁰ into Na⁺ and Cl⁻ (eq. 11) via:

$$x_{\text{NaCl}\pm} = \Lambda_{\epsilon} / \Lambda_e \quad (\text{C1})$$

841 where $x_{\text{NaCl}\pm}$ is the fraction of NaCl dissolved as NaCl \pm , Λ_{ϵ} is the experimen-
842 tally determined equivalent conductance and Λ_e is the equivalent conductance of
843 a hypothetical completely dissociated NaCl solution of the same effective ionic
844 strength (Oelkers and Helgeson, 1988). Λ_e is calculated from the limiting equiva-
845 lent conductance of the electrolyte (Λ_e^0). Λ_e for NaCl solutions has been obtained
846 with the equation of Monica et al. (1984), which is valid up to at least 6 molal:

$$\Lambda_e \eta / \eta_0 = \left(\Lambda_e^0 - \frac{B_2 \sqrt{c}}{1 + B_2 \dot{a} \sqrt{c}} \right) \left(1 - \frac{B_1 \sqrt{c}}{1 + B_1 \dot{a} \sqrt{c}} \frac{e^{0.2929 \kappa \alpha} - 1}{0.2929 \kappa \alpha} \right) \quad (\text{C2})$$

847 where η is the viscosity of the solution, η_0 the viscosity of the pure solvent, c
848 the concentration of NaCl and \dot{a} the ion size parameter taken from Helgeson et al.
849 (1981). B_1 and B_2 are coefficients originating from the formula of Onsager (1927)
850 and modified by Monica et al. (1984) such as $B_1 = 8.2053 * 10^5 \sqrt{\rho} / (\epsilon T)^{3/2}$ and
851 $B_2 = 82.48 \sqrt{\rho} / (\eta \sqrt{\epsilon T})$, with ρ density of the solvent and ϵ dielectric constant
852 of water. $\kappa \alpha$ is a dimensionless quantity from the Debye-Huckel formula and is
853 calculated as:

$$\kappa \alpha = B_2 \dot{a} \sqrt{c} = 50.294 \dot{a} \sqrt{c} / \sqrt{\epsilon T} \quad (\text{C3})$$

854 Equation C2 is a refinement of the Wishaw and Stokes (1954) equation which
855 allows correction of the ionic mobility for changing viscosity and is based on
856 the original equations proposed for dilute solutions by Falkenhagen et al. (1952).

857 Oelkers and Helgeson (1988) have used the Shedlovsky equation (Shedlovsky,
858 1938) to estimate the degree of association in solutions up to 0.1 molal for various
859 electrolytes. However, the Shedlovsky equation is not valid for the calculation of
860 Λ_e for solutions containing more than about 0.1m. For some high-temperature
861 conditions, the calculated values of Λ_e are less than the observed Λ_e , leading to
862 $x_{\text{NaCl}\pm} > 1$.

863 Λ_e has been calculated for the data of Bianchi et al. (1989, 25°C, 1 bar, 0.5-3.6
864 molal), Chambers et al. (1956) (25°C, 1 bar, 0.1-5.35 molal) and from Quist and
865 Marshall (1968) for solutions of 0.1molal NaCl in the range 100°C-600°C. For
866 each experimental result, η_0 has been calculated with the IAPWS EOS of water.
867 When not measured, η was calculated with the equation of Mao et al. (2009). The
868 increase in viscosity for solutions of 0.1 molal NaCl or less has little impact on the
869 calculated Λ_e and has been neglected for the data of Quist and Marshall (1968).
870 The densities reported along with temperatures by Quist and Marshall (1968) were
871 individually converted to pressures with the IAPWS EOS.

872 **APPENDIX D**

873 The following tables provide values and covariance matrices for coefficients
874 used in the modeling and described in the text. The diagonal of a covariance
875 matrix is the variance.

ACCEPTED MANUSCRIPT

	Value	k_1	k_2	k_3	k_4	k_5	k_6	k_7	k_8	k_9	k_{10}	k_{11}	k_{12}	k_{13}	k_{14}	k_{15}	k_{16}	k_{17}	k_{18}	k_{19}	k_{20}	k_{21}
k_1	-	-	-	-	-	-	-	-	-	-	-	-	-	-	-	-	-	-	-	-	-	-
k_2	3.5237E-05	-3.14E-11	-1.32E-13	2.09E-16	-4.74E-09	7.14E-11	-4.48E-13	4.90E-16	-	-	-4.11E-08	6.68E-10	9.48E-12	-3.84E-14	4.98E-17	-	-	-4.58E-14	6.92E-17	-4.63E-12	1.15E-17	-
k_3	-1.3772E-07	-1.32E-13	5.69E-16	-9.10E-19	1.78E-11	-2.67E-13	1.68E-15	-1.76E-18	-	-	1.64E-10	-2.91E-12	-3.93E-14	1.62E-16	-2.14E-19	-	-	1.77E-16	-2.57E-19	1.93E-14	-4.54E-20	-
k_4	2.2366E-10	-2.09E-16	-9.10E-19	1.48E-21	-2.79E-14	4.19E-16	-2.63E-18	2.73E-21	-	-	-2.51E-13	4.58E-15	6.22E-17	-2.57E-19	3.47E-22	-	-	-2.78E-19	4.01E-22	-3.03E-17	6.90E-23	-
k_5	-2.7484E-02	-4.74E-09	1.78E-11	-2.79E-14	1.13E-06	-1.68E-08	1.04E-10	-1.31E-13	-	-	9.14E-06	-6.92E-08	-1.48E-09	5.65E-12	-7.04E-15	-	-	9.59E-12	-1.66E-14	6.64E-10	-2.01E-15	-
k_6	2.8638E-04	-7.14E-11	-2.67E-13	4.19E-16	-1.68E-08	2.58E-10	-1.61E-12	2.01E-15	-	-	-1.16E-07	1.16E-09	2.23E-11	-8.49E-14	1.05E-16	-	-	-1.48E-13	2.56E-16	-1.05E-11	3.19E-17	-
k_7	-1.3932E-06	-4.48E-13	1.68E-15	-2.63E-18	1.04E-10	-1.61E-12	1.00E-14	-1.25E-17	-	-	7.08E-10	-7.37E-12	-1.40E-13	5.32E-16	-6.57E-19	-	-	9.29E-16	-1.60E-18	6.62E-14	2.00E-19	-
k_8	1.7538E-09	-4.90E-16	-1.76E-18	2.73E-21	-1.31E-13	2.01E-15	-1.25E-17	1.61E-20	-	-	-9.04E-13	6.79E-15	1.54E-16	-5.74E-19	6.96E-22	-	-	-1.13E-18	2.01E-21	-7.05E-17	2.31E-22	-
k_9	-	-	-	-	-	-	-	-	-	-	-	-	-	-	-	-	-	-	-	-	-	-
k_{10}	-	-	-	-	-	-	-	-	-	-	-	-	-	-	-	-	-	-	-	-	-	-
k_{11}	2.5909E-02	-4.11E-08	1.64E-10	-2.51E-13	9.14E-06	-1.16E-07	7.08E-10	-9.04E-13	-	-	1.40E-04	-3.74E-07	-1.24E-08	4.89E-11	-6.33E-14	-	-	6.34E-11	-1.12E-13	4.30E-09	-1.23E-14	-
k_{12}	7.8597E-04	-6.68E-10	-2.91E-12	4.58E-15	-6.92E-08	1.16E-09	-7.37E-12	6.79E-15	-	-	-3.74E-07	1.99E-08	1.90E-10	-7.99E-13	1.03E-15	-	-	-8.33E-13	1.10E-15	-1.12E-10	2.66E-16	-
k_{13}	9.7084E-06	-9.48E-12	-3.93E-14	6.22E-17	-1.48E-09	2.23E-11	-1.40E-13	1.54E-16	-	-	-1.24E-08	1.90E-10	2.95E-12	-1.18E-14	1.52E-17	-	-	-1.42E-14	2.16E-17	-1.40E-12	3.49E-18	-
k_{14}	-4.1348E-08	-3.84E-14	1.62E-16	-2.57E-19	5.65E-12	-8.49E-14	5.32E-16	-5.74E-19	-	-	4.89E-11	-7.99E-13	-1.18E-14	4.78E-17	-6.22E-20	-	-	5.49E-17	-8.19E-20	5.65E-15	-1.38E-20	-
k_{15}	5.2823E-11	-4.98E-17	-2.14E-19	3.47E-22	-7.04E-15	1.05E-16	-6.57E-19	6.96E-22	-	-	-6.33E-14	1.03E-15	1.52E-17	-6.22E-20	8.31E-23	-	-	-6.85E-20	1.01E-22	-7.18E-18	1.67E-23	-
k_{16}	-	-	-	-	-	-	-	-	-	-	-	-	-	-	-	-	-	-	-	-	-	-
k_{17}	-	-	-	-	-	-	-	-	-	-	-	-	-	-	-	-	-	-	-	-	-	-
k_{18}	-9.7539E-08	-4.58E-14	1.77E-16	-2.78E-19	9.59E-12	-1.48E-13	9.29E-16	-1.13E-18	-	-	6.34E-11	-8.33E-13	-1.42E-14	5.49E-17	-6.85E-20	-	-	8.83E-17	-1.47E-19	6.89E-15	-1.98E-20	-
k_{19}	1.8277E-10	-6.92E-17	-2.57E-19	4.01E-22	-1.66E-14	2.56E-16	-1.60E-18	2.01E-21	-	-	-1.12E-13	1.10E-15	2.16E-17	-8.19E-20	1.01E-22	-	-	-1.47E-19	2.55E-22	-1.02E-17	3.13E-23	-
k_{20}	-5.7627E-06	-4.63E-12	1.93E-14	-3.03E-17	6.64E-10	-1.05E-11	6.62E-14	-7.05E-17	-	-	4.30E-09	-1.12E-10	-1.40E-12	5.65E-15	-7.18E-18	-	-	6.89E-15	-1.02E-17	7.39E-13	-1.86E-18	-
k_{21}	2.2035E-11	-1.15E-17	-4.54E-20	6.90E-23	-2.01E-15	3.19E-17	-2.00E-19	2.31E-22	-	-	-1.23E-14	2.66E-16	3.49E-18	-1.38E-20	1.67E-23	-	-	-1.98E-20	3.13E-23	-1.86E-18	5.32E-24	-

Table D1: Values of parameters and associated covariance matrix for equations 8 and 9 for $W_{\text{H}_2\text{O-CO}_2}/RT$.

	Value	j_1	j_2	j_3	j_4	j_5	j_6	j_7	j_8	j_9	j_{10}	j_{11}	j_{12}	j_{13}	j_{14}	j_{15}	j_{16}	j_{17}	j_{18}	j_{19}	j_{20}	j_{21}
j_1	4.5946E-02	8.70E-05	1.19E-06	9.89E-10	-9.97E-13	-	1.82E-08	-6.80E-11	6.69E-14	-9.86E-08	4.14E-12	5.24E-04	-8.27E-05	1.08E-06	-	-	-2.75E-06	3.08E-09	-	6.68E-15	4.02E-07	-
j_2	-7.6283E-04	1.19E-06	2.54E-08	1.90E-11	-1.79E-14	-	1.35E-10	-3.18E-13	1.31E-16	-9.90E-10	9.06E-14	2.42E-05	-1.78E-06	2.23E-08	-	-	-1.62E-07	2.92E-10	-	-1.92E-16	7.61E-09	-
j_3	-6.2299E-07	9.89E-10	1.90E-11	1.54E-14	-1.54E-17	-	1.11E-13	-2.68E-16	1.17E-19	-8.98E-13	-6.78E-17	1.76E-08	-1.34E-09	1.69E-11	-	-	-1.19E-10	2.19E-13	-	-1.51E-19	5.87E-12	-
j_4	6.1752E-10	-9.97E-13	-1.79E-14	-1.54E-17	1.59E-20	-	-1.17E-16	3.01E-19	-1.59E-22	9.45E-16	6.39E-20	-1.62E-11	1.28E-12	-1.61E-14	-	-	-1.10E-13	-2.03E-16	-	-1.37E-22	-5.67E-15	-
j_5	-	-	-	-	-	-	-	-	-	-	-	-	-	-	-	-	-	-	-	-	-	-
j_6	-4.5659E-05	1.82E-08	1.35E-10	1.11E-13	-1.17E-16	-	9.01E-12	-4.10E-14	4.80E-17	-2.54E-11	-4.39E-16	2.93E-07	-7.97E-09	1.25E-10	-	-	-2.82E-09	-7.17E-12	-	-1.27E-17	5.50E-11	-
j_7	1.4810E-07	-6.80E-11	-3.18E-13	-2.68E-16	3.01E-19	-	-4.10E-14	1.92E-16	-2.31E-19	1.04E-13	9.46E-19	1.76E-09	1.38E-11	-3.08E-13	-	-	-1.62E-11	3.98E-14	-	-6.63E-20	-1.53E-13	-
j_8	-1.3101E-10	6.69E-14	1.31E-16	1.17E-19	-1.59E-22	-	4.80E-17	-2.31E-19	2.81E-22	-1.11E-16	-2.43E-22	-2.42E-12	2.31E-15	1.45E-16	-	-	-2.18E-14	-5.29E-17	-	-8.55E-23	9.73E-17	-
j_9	4.3745E-05	-9.86E-08	-9.90E-10	-8.98E-13	9.45E-16	-	-2.54E-11	1.04E-13	1.11E-16	1.29E-10	3.38E-15	2.51E-07	6.51E-08	-9.27E-10	-	-	-3.18E-09	9.58E-12	-	-2.33E-17	-3.58E-10	-
j_{10}	2.7152E-09	-4.14E-12	-9.06E-14	-6.78E-17	6.39E-20	-	-4.39E-16	9.46E-19	-2.43E-22	3.38E-15	3.24E-19	-8.68E-11	6.31E-12	-7.93E-14	-	-	-5.84E-13	-1.06E-15	-	-7.35E-22	-2.69E-14	-
j_{11}	-6.3984E-01	5.24E-04	2.42E-05	1.76E-08	-1.62E-11	-	-2.93E-07	1.76E-09	-2.42E-12	2.51E-07	-8.68E-11	5.95E-02	-2.03E-03	2.11E-05	-	-	-4.51E-04	9.48E-07	-	-1.15E-12	7.51E-06	-
j_{12}	5.5016E-02	-8.27E-05	-1.78E-06	-1.34E-09	1.28E-12	-	-7.97E-09	1.38E-11	2.31E-15	6.51E-08	6.31E-12	-2.03E-03	1.30E-04	-1.57E-06	-	-	-1.39E-05	-2.59E-08	-	-2.03E-14	-5.53E-07	-
j_{13}	-6.7895E-04	1.08E-06	2.23E-08	1.69E-11	-1.61E-14	-	-1.25E-10	-3.08E-13	1.45E-16	-9.27E-10	-7.93E-14	2.11E-05	-1.57E-06	1.96E-08	-	-	-1.41E-07	2.54E-10	-	-1.64E-16	6.75E-09	-
j_{14}	-	-	-	-	-	-	-	-	-	-	-	-	-	-	-	-	-	-	-	-	-	-
j_{15}	-	-	-	-	-	-	-	-	-	-	-	-	-	-	-	-	-	-	-	-	-	-
j_{16}	5.2944E-03	-2.75E-06	-1.62E-07	-1.19E-10	1.10E-13	-	-2.82E-09	-1.62E-11	2.18E-14	-3.18E-09	5.84E-13	4.51E-04	1.39E-05	-1.41E-07	-	-	-3.51E-06	-7.58E-09	-	-9.71E-15	-5.02E-08	-
j_{17}	-1.1929E-05	3.08E-09	2.92E-10	2.19E-13	-2.03E-16	-	-7.17E-12	3.98E-14	-5.29E-17	9.58E-12	-1.06E-15	9.48E-07	-2.59E-08	2.54E-10	-	-	-7.58E-09	1.68E-11	-	-2.26E-17	9.09E-11	-
j_{18}	-	-	-	-	-	-	-	-	-	-	-	-	-	-	-	-	-	-	-	-	-	-
j_{19}	1.4402E-11	6.68E-15	-1.92E-16	-1.51E-19	1.37E-22	-	-1.27E-17	-6.63E-20	8.55E-23	-2.33E-17	7.35E-22	-1.15E-12	2.03E-14	-1.64E-16	-	-	-9.71E-15	-2.26E-17	-	-3.34E-23	-5.86E-17	-
j_{20}	-2.5360E-04	4.02E-07	7.61E-09	5.87E-12	-5.67E-15	-	-5.50E-11	-1.53E-13	9.73E-17	-3.58E-10	-2.69E-14	7.51E-06	-5.53E-07	6.75E-09	-	-	-5.02E-08	9.09E-11	-	-5.86E-17	2.43E-09	-
j_{21}	-	-	-	-	-	-	-	-	-	-	-	-	-	-	-	-	-	-	-	-	-	-

Table D2: Values of parameters and associated covariance matrix for equations 8 and 9 for α_{CO_2} .

	Value	C_1	C_2	C_3	C_4	C_5	C_6	C_7	C_8	C_9	C_{10}	C_{11}	C_{12}	C_{13}	C_{14}	C_{15}	C_{16}
C_1	-3.67E+00	1.12E+00	-2.26E-04	-2.84E-03	-8.47E-05	5.16E-04	1.22E-04	-1.38E-06	1.81E-01	1.74E-03	2.37E-05	-4.56E-02	-6.69E-04	-3.57E-03	9.14E-06	-8.39E-07	3.04E-08
C_2	-1.38E-03	-2.26E-04	1.63E-07	5.74E-07	7.06E-08	9.23E-07	-1.24E-07	-2.23E-09	-6.06E-05	-3.14E-07	-5.16E-09	8.12E-06	1.21E-07	2.44E-06	-6.30E-09	-8.19E-11	1.54E-11
C_3	8.92E-03	-2.84E-03	5.74E-07	7.22E-06	2.15E-07	-1.31E-06	-3.11E-07	3.50E-09	-4.60E-04	-4.42E-06	-6.03E-08	1.16E-04	1.70E-06	9.09E-06	-2.33E-08	2.13E-09	-7.74E-11
C_4	7.20E-04	-8.47E-05	7.06E-08	2.15E-07	3.11E-08	5.34E-07	-5.49E-08	-1.30E-09	-2.38E-05	-1.09E-07	-1.98E-09	1.28E-06	5.20E-08	1.00E-06	-2.60E-09	-4.12E-11	7.38E-12
C_5	1.00E+00	5.16E-04	9.23E-07	-1.31E-06	5.34E-07	2.33E-04	-7.21E-07	-5.84E-07	-8.56E-04	4.81E-05	-6.87E-07	-1.60E-03	-1.62E-06	5.38E-05	-1.44E-07	-5.52E-09	-2.69E-10
C_6	-4.23E-04	1.22E-04	-1.24E-07	-3.11E-07	-5.49E-08	-7.21E-07	1.01E-07	1.73E-09	3.67E-05	2.00E-07	1.98E-09	-3.20E-06	-9.09E-08	-1.66E-06	4.30E-09	8.70E-11	-2.32E-11
C_7	-1.53E-03	-1.38E-06	-2.23E-09	3.50E-09	-1.30E-09	-5.84E-07	1.73E-09	1.48E-09	2.59E-06	-1.22E-07	1.75E-09	4.06E-06	1.80E-09	-1.60E-07	4.16E-10	1.43E-11	7.22E-13
C_8	-9.85E+00	1.81E-01	-6.06E-05	-4.60E-04	-2.38E-05	-8.56E-04	3.67E-05	2.59E-06	1.17E-01	3.45E-04	5.12E-06	2.89E-04	-3.97E-04	-5.56E-03	1.38E-05	1.03E-07	-5.21E-10
C_9	-4.18E-02	1.74E-03	-3.14E-07	-4.42E-06	-1.09E-07	4.81E-05	2.00E-07	-1.22E-07	3.45E-04	4.94E-05	-6.20E-07	-1.94E-04	-5.10E-06	-7.13E-06	1.80E-08	-2.44E-09	-1.90E-12
C_{10}	1.99E-04	2.37E-05	-5.16E-09	-6.03E-08	-1.98E-09	-6.87E-07	1.98E-09	1.75E-09	5.12E-06	-6.20E-07	9.84E-09	1.11E-06	3.80E-08	-1.72E-07	4.35E-10	5.02E-12	1.73E-12
C_{11}	-6.14E-01	-4.56E-02	8.12E-06	1.16E-04	1.28E-06	-1.60E-03	-3.20E-06	4.06E-06	2.89E-04	-1.94E-04	1.11E-06	6.57E-02	2.24E-06	-2.68E-04	6.88E-07	5.53E-08	1.80E-09
C_{12}	3.16E-02	-6.69E-04	1.21E-07	1.70E-06	5.20E-08	-1.62E-06	-9.09E-08	1.80E-09	-3.97E-04	-5.10E-06	3.80E-08	2.24E-06	3.37E-06	1.81E-05	-4.43E-08	5.62E-10	2.15E-11
C_{13}	8.70E-01	-3.57E-03	2.44E-06	9.09E-06	1.00E-06	5.38E-05	-1.66E-06	-1.60E-07	-5.56E-03	-7.13E-06	-1.72E-07	-2.68E-04	1.81E-05	2.95E-04	-7.34E-07	-1.13E-08	2.90E-10
C_{14}	-5.60E-04	9.14E-06	-6.30E-09	-2.33E-08	-2.60E-09	-1.44E-07	4.30E-09	4.16E-10	1.38E-05	1.80E-08	4.35E-10	6.88E-07	-4.43E-08	-7.34E-07	1.83E-09	2.86E-11	-7.65E-13
C_{15}	2.80E-06	-8.39E-07	-8.19E-11	2.13E-09	-4.12E-11	-5.52E-09	8.70E-11	1.43E-11	1.03E-07	-2.44E-09	5.02E-12	5.53E-08	5.62E-10	-1.13E-08	2.86E-11	2.01E-12	-5.29E-14
C_{16}	6.48E-08	3.04E-08	1.54E-11	-7.74E-11	7.38E-12	-2.69E-10	-2.32E-11	7.22E-13	-5.21E-10	-1.90E-12	1.73E-12	1.80E-09	2.15E-11	2.90E-10	-7.65E-13	-5.29E-14	2.66E-14

Table D3: Values and covariance matrices for C_1 to C_{16} (equations 13 to 16).

	Value	D_1	D_2	D_3	D_4	D_5
D_1	5.046E01	8.15E00	-9.42E-01	-2.89E-02	5.76E-03	-1.41E-01
D_2	-3.533E00	-9.42E-01	2.69E-01	1.64E-03	-3.91E-04	-9.28E-03
D_3	-1.525E-01	-2.89E-02	1.64E-03	1.22E-04	-2.38E-05	7.87E-04
D_4	2.307E-02	5.76E-03	-3.91E-04	-2.38E-05	4.73E-06	-1.52E-04
D_5	-4.801E-01	-1.41E-01	-9.28E-03	7.87E-04	-1.52E-04	7.02E-03

Table D4: Values and covariance matrices for D_1 to D_5 (equation 17).

876 **References**

- 877 Adams L.H. (1931) Equilibrium in Binary Systems Under Pressure. I. An Ex-
878 perimental and Thermodynamic Investigation of the System NaCl-H₂O, at 25
879 degrees. *Journal of American Chemical Society* **53**, 3769–3813.
- 880 Akinfiyev N.N. and Diamond L.W. (2010) Thermodynamic model of aqueous CO₂-
881 H₂O-NaCl solutions from -22 to 100 °C and from 0.1 to 100 MPa. *Fluid Phase*
882 *Equilibria* **295**, 104 – 124. doi:10.1016/j.fluid.2010.04.007.
- 883 Anderson G. and Crerar D. (1993) Thermodynamics in geochemistry: The equi-
884 librium model p. 588.
- 885 Anderson G., Castet S., Schott J. and Mesmer R. (1991) The density model
886 for estimation of thermodynamic parameters of reactions at high temperatures
887 and pressures. *Geochimica et Cosmochimica Acta* **55**, 1769 – 1779. doi:
888 10.1016/0016-7037(91)90022-W.
- 889 Anderson G.K. (2002) Solubility of carbon dioxide in water under incipient
890 clathrate formation conditions. *Journal of Chemical and Engineering Data*
891 **47**, 219–222. doi:10.1021/je015518c.
- 892 Angiboust S., Wolf S., Burov E., Agard P. and Yamato P. (2012) Effect of fluid
893 circulation on subduction interface tectonic processes: Insights from thermo-
894 mechanical numerical modelling. *Earth and Planetary Science Letters* **357-**
895 **358**, 238 – 248. doi:10.1016/j.epsl.2012.09.012.
- 896 Aranovich L. and Newton R. (1996) H₂O activity in concentrated NaCl solutions
897 at high pressures and temperatures measured by the brucite-periclase equilib-
898 rium. *Contributions to Mineralogy and Petrology* **125**, 200–212.

- 899 Aranovich L.Y. and Berman R.G. (1996) Optimized standard state and solution
900 properties of minerals. *Contributions to Mineralogy and Petrology* **126**, 25–37.
901 10.1007/s004100050233.
- 902 Aranovich L.Y. and Newton R.C. (1999) Experimental determination of CO₂-H₂O
903 activity-composition relations at 600-1000 degrees C and 6-14 kbar by reversed
904 decarbonation and dehydration reactions. *American Mineralogist* **84**, 1319–
905 1332.
- 906 Bamberger A., Sieder G. and Maurer G. (2000) High-pressure (vapor+liquid)
907 equilibrium in binary mixtures of (carbon dioxide+water or acetic acid) at tem-
908 peratures from 313 to 353 K. *The Journal of Supercritical Fluids* **17**, 97 – 110.
909 doi:10.1016/S0896-8446(99)00054-6.
- 910 Bartholomé E. and Friz H. (1956) Solubility of CO₂ in water. *Chem. Ing. Tech.* .
911 **28**, 706–708.
- 912 Becker J.A., Bickle M.J., Galy A. and Holland T.J. (2008) Himalayan metamor-
913 phic CO₂ fluxes: Quantitative constraints from hydrothermal springs. *Earth*
914 *and Planetary Science Letters* **265**, 616 – 629. doi:10.1016/j.epsl.2007.10.046.
- 915 Berman R. (1988) Internally-consistent thermodynamic data for minerals in the
916 system Na₂O-K₂O-CaO-MgO-FeO-Fe₂O₃-Al₂O₃-SiO₂-TiO₂-H₂O-CO₂. *Jour-*
917 *nal of Petrology* **29**, 445–522.
- 918 Berman R.G. and Aranovich L.Y. (1996) Optimized standard state and solution
919 properties of minerals. *Contributions to Mineralogy and Petrology* **126**, 1–24.
920 10.1007/s004100050232.

- 921 Bevington P. and Robinson D. (2002) *Data Reduction and Error Analysis for The*
922 *Physical Sciences*. McGraw-Hill Higher Education, 3 edn.
- 923 Bianchi H., Corti H.R. and Fernandez-Prini R. (1989) The conductivity of con-
924 centrated aqueous mixtures of NaCl and MgCl₂ at 25°C. *Journal of Solution*
925 *Chemistry* **18**, 485–491. doi:10.1007/BF00657336.
- 926 Bickle M.J. (2009) Geological carbon storage. *Nature Geoscience* **2**, 815–818.
927 doi:10.1038/ngeo687.
- 928 Bodnar R. (1994) Synthetic fluid inclusions: XII. The system H₂O-NaCl. Experi-
929 mental determination of the halite liquidus and isochores for a 40 wt% NaCl so-
930 lution. *Geochimica et Cosmochimica Acta* **58**, 1053 – 1063. doi:10.1016/0016-
931 7037(94)90571-1.
- 932 Chambers J.F., Stokes J.M. and Stokes R.H. (1956) Conductances of Concentrated
933 Aqueous Sodium and Potassium Chloride Solutions at 25°C. *The Journal of*
934 *Physical Chemistry* **60**, 985–986. doi:10.1021/j150541a040.
- 935 Chapman W., Gubbins K., Jackson G. and Radosz M. (1989) SAFT: Equation-of-
936 state solution model for associating fluids. *Fluid Phase Equilibria* **52**, 31 – 38.
937 doi:10.1016/0378-3812(89)80308-5.
- 938 Chester F., Evans J. and Biegel R. (1993) Internal Structure and Weakening Mech-
939 anisms Of The San-Andreas Fault. *Journal of Geophysical Research-Solid*
940 *Earth* **98**, 771–786.
- 941 Clegg S.L. and Pitzer K.S. (1992) Thermodynamics of multicomponent, misci-
942 ble, ionic solutions: generalized equations for symmetrical electrolytes. *The*
943 *Journal of Physical Chemistry* **96**, 3513–3520. doi:10.1021/j100187a061.

- 944 Clegg S.L., Pitzer K.S. and Brimblecombe P. (1992) Thermodynamics of mul-
945 ticomponent, miscible, ionic solutions. Mixtures including unsymmetrical
946 electrolytes. *The Journal of Physical Chemistry* **96**, 9470–9479. doi:
947 10.1021/j100202a074.
- 948 Clyne M.A., Potter R.W. and Haas J.L. (1981) Solubility of sodium chloride in
949 aqueous electrolyte solutions from 10 to 100 degrees C. *Journal of Chemical*
950 *& Engineering Data* **26**, 396–398. doi:10.1021/je00026a014.
- 951 Connolly J.A.D. (2009) The geodynamic equation of state: What and how. *Geo-*
952 *chemistry Geophysics Geosystems* **10**. doi:10.1029/2009GC002540.
- 953 De Capitani C. and Peters T. (1982) Corresponding states in binary solutions and
954 graphical determination of Margules parameters. *Contributions to Mineralogy*
955 *and Petrology* **81**, 48–58.
- 956 De Capitani C. and Petrakakis K. (2010) The computation of equilibrium assem-
957 blage diagrams with Theriak/Domino software. *American Mineralogist* **95**,
958 1006–1016. doi:10.2138/am.2010.3354.
- 959 Debye P. and Hückel E. (1923a) The theory of electrolytes I. The lowering of the
960 freezing point and related occurrences. *Physikalische Zeitschrift* **24**, 185–206.
- 961 Debye P. and Hückel E. (1923b) The theory of the electrolyte II - The border law
962 for electrical conductivity. *Physikalische Zeitschrift* **24**, 305–325.
- 963 Diamond L.W. and Akinfiyev N.N. (2003) Solubility of CO₂ in water from -1.5 to
964 100 °C and from 0.1 to 100 MPa: evaluation of literature data and thermody-
965 namic modelling. *Fluid Phase Equilibria* **208**, 265 – 290. doi:10.1016/S0378-
966 3812(03)00041-4.

- 967 Driesner T. (2007) The system H₂O-NaCl. Part II: Correlations for molar vol-
968 ume, enthalpy, and isobaric heat capacity from 0 to 1000°C, 1 to 5000 bar,
969 and 0 to 1 XNaCl. *Geochimica et Cosmochimica Acta* **71**, 4902 – 4919. doi:
970 10.1016/j.gca.2007.05.026.
- 971 Driesner T. and Heinrich C.A. (2007) The system H₂O-NaCl. Part I: Correlation
972 formulae for phase relations in temperature-pressure-composition space from
973 0 to 1000°C, 0 to 5000 bar, and 0 to 1 XNaCl. *Geochimica et Cosmochimica*
974 *Acta* **71**, 4880 – 4901. doi:10.1016/j.gca.2006.01.033.
- 975 Drummond S. (1981) *Boiling and mixing of hydrothermal fluids : chemical effects*
976 *on mineral precipitation*. Ph.D. thesis, Pennsylvania States University.
- 977 Duan Z. and Li D. (2008) Coupled phase and aqueous species equilibrium of the
978 H₂O-CO₂-NaCl-CaCO₃ system from 0 to 250 °C, 1 to 1000 bar with NaCl
979 concentrations up to saturation of halite. *Geochimica et Cosmochimica Acta*
980 **72**, 5128 – 5145. doi:10.1016/j.gca.2008.07.025.
- 981 Duan Z. and Sun R. (2003) An improved model calculating CO₂ solubility in pure
982 water and aqueous NaCl solutions from 273 to 533 K and from 0 to 2000 bar.
983 *Chemical Geology* **193**, 257 – 271. doi:10.1016/S0009-2541(02)00263-2.
- 984 Duan Z. and Zhang Z. (2006) Equation of state of the H₂O-CO₂ system up to
985 10 GPa and 2573K: Molecular dynamics simulations with ab initio potential
986 surface. *Geochimica et Cosmochimica Acta* **70**, 2311–2324.
- 987 Duan Z., Møller N. and Weare J.H. (1992) An equation of state for the CH₄-CO₂-
988 H₂O system: II. Mixtures from 50 to 1000°C and 0 to 1000 bar. *Geochimica et*
989 *Cosmochimica Acta* **56**, 2619 – 2631. doi:10.1016/0016-7037(92)90348-M.

990 Duan Z., Møller N. and Weare J.H. (1995) Equation of state for the NaCl-
991 H₂O-CO₂ system: prediction of phase equilibria and volumetric properties.
992 *Geochimica et Cosmochimica Acta* **59**, 2869 – 2882. doi:10.1016/0016-
993 7037(95)00182-4.

994 Duan Z., Møller N. and Weare J. (1996) A general equation of state for super-
995 critical fluids and molecular dynamics simulation of mixture PVTX properties.
996 *Geochimica et Cosmochimica Acta* **60**, 1209–1216.

997 Duan Z., Møller N. and Weare J. (2000) Accurate prediction of thermodynamic
998 properties of fluids in the system H₂O-CO₂-CH₄-N₂. *Geochimica et Cos-*
999 *mochimica Acta* **64**, 1069–1075. doi:10.1016/S0016-7037(99)00368-3.

1000 Duan Z., Møller N. and Weare J. (2003) Equations of State for the NaCl-H₂O-CH₄
1001 System and the NaCl-H₂O-CO₂-CH₄ System: Phase Equilibria and Volumetric
1002 Properties above 573 K. *Geochimica et Cosmochimica Acta* **67**, 671–680. doi:
1003 10.1016/S0016-7037(02)01226-7.

1004 Duan Z., Sun R. and Zhu C. (2006) An improved model for the calculation of
1005 CO₂ solubility in aqueous solutions containing Na⁺, K⁺, Ca²⁺, Mg²⁺, Cl⁻, and
1006 SO₄²⁻. *Marine Chemistry* **98**, 131–139. doi:10.1016/j.marchem.2005.09.001.

1007 Duan Z., Hu J., Li D. and Mao S. (2008) Densities of the CO₂-H₂O and CO₂-H₂O-
1008 NaCl Systems Up to 647 K and 100 MPa. *Energy & Fuels* **22**, 1666–1674.

1009 Edmond J., Measures C., McDuff R., Chan L., Collier R., Grant B., Gordon L.
1010 and Corliss J. (1979) Ridge crest hydrothermal activity and the balances of
1011 the major and minor elements in the ocean: The Galapagos data. *Earth and*
1012 *Planetary Science Letters* **46**, 1 – 18. doi:10.1016/0012-821X(79)90061-X.

- 1013 Ellis A. and Golding R. (1963) Solubility of carbon dioxide above 100°C in water
1014 and in sodium chloride solutions. *American Journal of Science* **261**, 47–60.
- 1015 Evans K. and Powell R. (2006) A method for activity calculations in saline and
1016 mixed solvent solutions at elevated temperature and pressure: A framework for
1017 geological phase equilibria calculations. *Geochimica et cosmochimica acta* **70**,
1018 **22**, pp. 5488–5506. doi:10.1016/j.gca.2006.08.032.
- 1019 Evans K. and Powell R. (2007) DES-code: A metacode to aid calculation of the
1020 chemical potential of aqueous solutions at elevated temperatures and pressures.
1021 *Computers and Geosciences* **33**, 789–807. doi:10.1016/j.cageo.2006.09.010.
- 1022 Evans K.A., Powell R. and Holland T.J.B. (2010) Internally consistent data
1023 for sulphur-bearing phases and application to the construction of pseudosec-
1024 tions for mafic greenschist facies rocks in Na₂O-CaO-K₂O-FeO-MgO-Al₂O₃-
1025 SiO₂-CO₂-O-S-H₂O. *Journal of Metamorphic Geology* **28**, 667–687. doi:
1026 10.1111/j.1525-1314.2010.00890.x.
- 1027 Falkenhagen H., Leist M. and Kelbg G. (1952) Zur Theorie der Leitfähigkeit
1028 starker nicht assoziierender Elektrolyte bei hheren Konzentrationen. *Annalen
1029 der Physik* **446**, 51–59. doi:10.1002/andp.19524460110.
- 1030 Farelo F., Vonbrachel G. and Offermann H. (1993) Solid liquid equilibria in the
1031 ternary system NaCl-KCl-H₂O. *Canadian Journal of Chemical Engineering*
1032 **71**, 141–146.
- 1033 Ferry J.M. (1984) A Biotite Isograd in South-Central Maine, U.S.A.: Mineral
1034 Reactions, Fluid Transfer, and Heat Transfer. *Journal of Petrology* **25**, 871–
1035 893. doi:10.1093/petrology/25.4.871.

- 1036 Flowers G.C. (1979) Correction of Holloway's (1977) adaptation of the modified
1037 Redlich-Kwong equation of state for calculation of the fugacities of molecular
1038 species in supercritical fluids of geologic interest. *Contributions to Mineralogy
1039 and Petrology* **69**, 315–318. doi:10.1007/BF00372333.
- 1040 García A., Thomsen K. and Stenby E. (2006) Prediction of mineral scale for-
1041 mation in geothermal and oilfield operations using the Extended UNIQUAC
1042 model: Part II. Carbonate-scaling minerals. *Geothermics* **35**, 239 – 284. doi:
1043 10.1016/j.geothermics.2006.03.001.
- 1044 Gillespie P. and Wilson G. (1982) Vaporliquid and liquidliquid equilibria:
1045 watermethane, watercarbon dioxide, waterhydrogen sulfide, watern-pentane,
1046 watermethanen-pentane. *Gas Processors Association, Tulsa, Research Report
1047 RR48* .
- 1048 Grant-Taylor D.F. (1981) Partial molar volumes of sodium chloride solutions at
1049 200 bar, and temperatures from 175 to 350°C. *Journal of Solution Chemistry*
1050 **10**, 621–630. doi:10.1007/BF00650738.
- 1051 Greenwood H. (1967) Wollastonite: Stability in H₂O-CO₂ mixtures and oc-
1052 currence in a contact-metamorphic aureole near Salmo, British Columbia,
1053 Canada. *American Mineralogist* **52**, 1669–1680.
- 1054 Guggenheim E. (1977) *Thermodynamics*. North-Holland Publishing Company,
1055 Amsterdam.
- 1056 Hacker B., Abers G. and Peacock S. (2003) Subduction factory - 1. Theoretical
1057 mineralogy, densities, seismic wave speeds, and H₂O contents. *Journal of Geo-
1058 physical Research - Solid Earth* **108**. doi:10.1029/2001JB001127.

- 1059 Hähnel O. (1920) Solubility of carbon dioxide in water. *Centr. Min. Geol.* **25**,
1060 25–32.
- 1061 Helgeson H.C., Kirkham D.H. and Flowers G.C. (1981) Theoretical prediction
1062 of the thermodynamic behavior of aqueous electrolytes at high pressures and
1063 temperatures: IV. Calculation of activity coefficients, osmotic coefficients, and
1064 apparent molal and standard and relative partial molal properties to 600C and
1065 5kb. *American Journal of Science* **281**, 1249–1516.
- 1066 Hnedkovský L., Wood R.H. and Majer V. (1996) Volumes of aqueous solutions of
1067 CH₄, CO₂, H₂S and NH₃ at temperatures from 298.15 K to 705 K and pressures
1068 to 35 MPa. *The Journal of Chemical Thermodynamics* **28**, 125 – 142. doi:
1069 10.1006/jcht.1996.0011.
- 1070 Holland T. and Powell R. (1991) A compensated Redlich-Kwong (CORK) equa-
1071 tion for volumes and fugacities of CO₂ and H₂O in the range 1 bar to 50 kbar
1072 and 100-1600 degrees C. *Contributions to Mineralogy and Petrology* **109**, 265–
1073 273.
- 1074 Holland T. and Powell R. (2003) Activity-composition relations for phases in
1075 petrological calculations: an asymmetric multicomponent formulation. *Con-
1076 tributions to Mineralogy and Petrology* **145**, **4**, 492–501. doi:10.1007/s00410-
1077 003-0464-z.
- 1078 Holland T.J.B. and Powell R. (1990) An enlarged and updated internally con-
1079 sistent thermodynamic dataset with uncertainties and correlations - the system
1080 K₂O-Na₂O-CaO-MgO-MnO-FeO-Fe₂O₃-Al₂O₃-TiO₂-SiO₂-C-H₂-O₂. *Journal
1081 of Metamorphic Geology* **8**, 89–124. doi:10.1111/j.1525-1314.1990.tb00458.x.

- 1082 Holland T.J.B. and Powell R. (1998) An internally consistent thermodynamic data
1083 set for phases of petrological interest. *Journal of Metamorphic Geology* **16**, **3**,
1084 309–343. doi:10.1111/j.1525-1314.1998.00140.x.
- 1085 Holland T.J.B. and Powell R. (2011) An improved and extended internally consis-
1086 tent thermodynamic dataset for phases of petrological interest, involving a new
1087 equation of state for solids. *Journal of Metamorphic Geology* **29**, 333–383.
1088 doi:10.1111/j.1525-1314.2010.00923.x.
- 1089 Houston S., Smalley C., Laycock A. and Yardley B.W. (2011) The relative impor-
1090 tance of buffering and brine inputs in controlling the abundance of Na and Ca
1091 in sedimentary formation waters. *Marine and Petroleum Geology* **28**, 1242 –
1092 1251. doi:10.1016/j.marpetgeo.2011.03.002.
- 1093 Hu J., Duan Z., Zhu C. and Chou I.M. (2007) PVTx properties of the CO₂-
1094 H₂O and CO₂-H₂O-NaCl systems below 647 K: Assessment of experimental
1095 data and thermodynamic models. *Chemical Geology* **238**, 249 – 267. doi:
1096 10.1016/j.chemgeo.2006.11.011.
- 1097 Ji X. and Zhu C. (2012) A SAFT equation of state for the quaternary H₂S-CO₂-
1098 H₂O-NaCl system. *Geochimica et Cosmochimica Acta* **91**, 40 – 59. doi:
1099 10.1016/j.gca.2012.05.023.
- 1100 Ji X., Tan S.P., Adidharma H. and Radosz M. (2005) SAFT1-RPM Approximation
1101 Extended to Phase Equilibria and Densities of CO₂-H₂O and CO₂-H₂O-NaCl
1102 Systems. *Industrial & Engineering Chemistry Research* **44**, 8419–8427. doi:
1103 10.1021/ie050725h.

- 1104 Johnson E.L. (1991) Experimentally determined limits for H₂O-CO₂-NaCl
1105 immiscibility in granulites. *Geology* **19**, 925–928. doi:10.1130/0091-
1106 7613(1991)019<0925:EDLFHO>2.3.CO;2.
- 1107 Joyce D.B. and Holloway J.R. (1993) An experimental determination of the ther-
1108 modynamic properties of H₂O-CO₂-NaCl fluids at high pressures and temper-
1109 atures. *Geochimica et Cosmochimica Acta* **57**, 733 – 746. doi:10.1016/0016-
1110 7037(93)90165-S.
- 1111 Keevil N.B. (1942) Vapor Pressures of Aqueous Solutions at High Temperatures.
1112 *Journal of the American Chemical Society* **64**, 841–850.
- 1113 Kerrick D.M. and Caldeira K. (1998) Metamorphic CO₂ degassing from orogenic
1114 belts. *Chemical Geology* **145**, 213 – 232. doi:10.1016/S0009-2541(97)00144-
1115 7.
- 1116 Kiepe J., Horstmann S., Fischer K. and Gmehling J. (2002) Experimental deter-
1117 mination and prediction of gas solubility data for CO₂ + H₂O mixtures con-
1118 taining NaCl or KCl at temperatures between 313 and 393 K and pressures
1119 up to 10 MPa. *Industrial & Engineering Chemistry Research* **41**, 4393–4398.
1120 doi:10.1021/ie020154i.
- 1121 King M.B., Mubarak A., Kim J.D. and Bott T.R. (1992) The mutual solubilities
1122 of water with supercritical and liquid carbon dioxides. *The Journal of Super-
1123 critical Fluids* **5**, 296 – 302. doi:10.1016/0896-8446(92)90021-B.
- 1124 Kritschewsky I., Shaworonkoff N. and Aepelbaum V. (1935) Combined solubility
1125 of gases in liquids under pressure I Solubility of carbon dioxide in water from
1126 its mixtures with hydrogen of 20 and 30 degrees C and total pressure of 30

- 1127 kg/cm²). *Zeitschrift Fur Physikalische Chemie-Abteilung A-Chemische Ther-*
1128 *modynamik Kinetik Elektrochemie Eigenschaftslehre* **175**, 232–238.
- 1129 Le Bayon R., de Capitani C. and Frey M. (2006) Modelling phase-assemblage di-
1130 agrams for magnesian metapelites in the system K₂O-FeO-MgO-Al₂O₃-SiO₂-
1131 H₂O: geodynamic consequences for the Monte Rosa nappe, Western Alps. *Con-*
1132 *tributions to Mineralogy and Petrology* **151**, 395–412. doi:10.1007/s00410-
1133 006-0067-6.
- 1134 Levenberg K. (1944) A Method for the Solution of Certain Non-Linear Problems
1135 in Least Squares. *The Quarterly of Applied Mathematics* **2**, 164–168.
- 1136 Li D. and Duan Z. (2007) The speciation equilibrium coupling with phase equi-
1137 librium in the H₂O-CO₂-NaCl system from 0 to 250 °C, from 0 to 1000 bar,
1138 and from 0 to 5 molality of NaCl. *Chemical Geology* **244**, 730 – 751. doi:
1139 10.1016/j.chemgeo.2007.07.023.
- 1140 Li Z., Dong M., Li S. and Dai L. (2004) Densities and Solubilities for Binary
1141 Systems of Carbon Dioxide + Water and Carbon Dioxide + Brine at 59°C and
1142 Pressures to 29 MPa. *Journal of Chemical & Engineering Data* **49**, 1026–1031.
1143 doi:10.1021/jc049945c.
- 1144 L'Vov S., Zarembo V. and Gilyarov V. (1981) High-precision study of vol-
1145 ume properties of water solutions of sodium-chloride under high parameters.
1146 *Geokhimiya* pp. 505–516.
- 1147 Malinin S. and Kurovskaya N. (1975) Investigation of CO₂ solubility in solutions
1148 of chlorides at elevated-temperatures and pressures of CO₂. *Geokhimiya* pp.
1149 547–550.

- 1150 Malinin S. and Saveleva N. (1972) Experimental investigations of CO₂ solubility
1151 in NaCl and CaCl₂ solutions at temperatures of 25, 50 and 75 degrees and
1152 elevated CO₂ pressure. *Geokhimiya* pp. 643–&.
- 1153 Mao S. and Duan Z. (2008) The P, V, T,x properties of binary aqueous chloride
1154 solutions up to T = 573 K and 100 MPa. *The Journal of Chemical Thermody-*
1155 *namics* **40**, 1046 – 1063. doi:10.1016/j.jct.2008.03.005.
- 1156 Mao S. and Duan Z. (2009) The Viscosity of Aqueous Alkali-Chloride Solutions
1157 up to 623 K, 1,000 bar, and High Ionic Strength. *International Journal of*
1158 *Thermophysics* **30**, 1510–1523. doi:10.1007/s10765-009-0646-7.
- 1159 Mao S., Duan Z. and Hu W. (2009) A vapor - liquid phase equilibrium model
1160 for binary CO₂ - H₂O and CH₄-H₂O systems above 523K for application
1161 to fluid inclusions. *The Journal of Supercritical Fluids* **50**, 13 – 21. doi:
1162 10.1016/j.supflu.2009.02.007.
- 1163 Markham A.E. and Kobe K.A. (1941) The Solubility of Carbon Dioxide and Ni-
1164 trous Oxide in Aqueous Salt Solutions. *Journal of American Chemical Society*
1165 **63**, 449–454.
- 1166 Marquardt D.W. (1963) An Algorithm for Least-Squares Estimation of Nonlinear
1167 Parameters. *Journal of the Society for Industrial and Applied Mathematics* **11**,
1168 pp. 431–441.
- 1169 Mather A. and Franck E. (1992) Phase-equilibria in the system carbon dioxide -
1170 water at elevated pressures. *Journal of Physical Chemistry* **96**, 6–8.
- 1171 Matous J., Sobr J., Novak J. and Pick J. (1969) Solubility of carbon dioxide in

- 1172 water at pressures up to 40 atm. *Collection of Czechoslovak Chemical Commu-*
1173 *nications* **34**, 3982–2985.
- 1174 Molnar P., England P. and Martinod J. (1993) Mantle dynamics, uplift of the Ti-
1175 betan plateau, and the Indian monsoon. *Reviews Of Geophysics* **31**, 357–396.
1176 doi:10.1029/93RG02030.
- 1177 Monica M.D., Ceglie A. and Agostiano A. (1984) A conductivity equation for
1178 concentrated aqueous solutions. *Electrochimica Acta* **29**, 933 – 937. doi:
1179 10.1016/0013-4686(84)87138-8.
- 1180 Müller G., Bender E. and Maurer G. (1988) Vapor-liquid-equilibrium in the
1181 ternary-system ammonia-carbon dioxide-water at high water contents in the
1182 range 373-K to 473-K. *Berichte der Bunsen-Gesellschaft-Physical Chemistry*
1183 *Chemical Physics* **92**, 148–160.
- 1184 Namiot A. (1991) Solubility of Gases in Water. *Nedra, Moscow* .
- 1185 Nesbitt H.W. and Markovics G. (1997) Weathering of granodioritic crust, long-
1186 term storage of elements in weathering profiles, and petrogenesis of silici-
1187 clastic sediments. *Geochimica et Cosmochimica Acta* **61**, 1653 – 1670. doi:
1188 10.1016/S0016-7037(97)00031-8.
- 1189 Newton R., Smith J. and Windley B. (1980) Carbonic metamorphism, granulites
1190 and crustal growth. *Nature* **288**, 45–50. doi:10.1038/288045a0.
- 1191 Nicollet C. and Goncalves P. (2005) Two contrasted P-T-time paths of coronitic
1192 metanorites of the French Massif Central: are reaction textures reliable guides
1193 to metamorphic histories? *Journal of Metamorphic Geology* **23**, 97–105. doi:
1194 10.1111/j.1525-1314.2005.00564.x.

- 1195 Nighswander J., Kalogerakis N. and Mehrotra A. (1989) Solubilities of carbon-
1196 dioxide in water and 1 wt-percent NaCl solution at pressures up to 10-mpa and
1197 temperatures from 80 degrees C to 200 degrees C. *Journal of Chemical and*
1198 *Engineering Data* **34**, 355–360.
- 1199 Oelkers E. and Helgeson H. (1993a) Multiple ion association in supercritical aque-
1200 ous solutions of single electrolytes. *Science* **261**, 888–891. Cited By (since
1201 1996) 61.
- 1202 Oelkers E.H. and Helgeson H.C. (1988) Calculation of the thermodynamic and
1203 transport properties of aqueous species at high pressures and temperatures: dis-
1204 sociation constants for supercritical alkali metal halides at temperatures from
1205 400 to 800°C and pressures from 500 to 4000 bar. *The Journal of Physical*
1206 *Chemistry* **92**, 1631–1639. doi:10.1021/j100317a049.
- 1207 Oelkers E.H. and Helgeson H.C. (1993b) Calculation of dissociation constants and
1208 the relative stabilities of polynuclear clusters of 1:1 electrolytes in hydrother-
1209 mal solutions at supercritical pressures and temperatures. *Geochimica et Cos-*
1210 *mochimica Acta* **57**, 2673 – 2697. doi:10.1016/0016-7037(93)90383-8.
- 1211 Oelkers E.H., Benezeth P. and Pokrovski G.S. (2009) Thermodynamic Databases
1212 for Water-Rock Interaction. In *THERMODYNAMICS AND KINETICS OF*
1213 *WATER-ROCK INTERACTION* (eds. E. Oelkers and J. Schott), Mineralogi-
1214 cal Society of America, vol. 70 of *Reviews in Mineralogy & Geochemistry*, pp.
1215 1–46. doi:10.2138/rmg.2009.70.1.
- 1216 Onsager L. (1927) On the theory of electrolytes. II. *Physikalische Zeitschrift* **28**,
1217 277–298.

- 1218 Pinho S.P. and Macedo E.A. (2005) Solubility of NaCl, NaBr, and KCl in Water,
1219 Methanol, Ethanol, and Their Mixed Solvents. *Journal of Chemical & Engi-*
1220 *neering Data* **50**, 29–32. doi:10.1021/je049922y.
- 1221 Pitzer K. (1973) Thermodynamics of electrolytes.1. Theoretical basis and general
1222 equations. *Journal of Physical Chemistry* **77**, 268–277.
- 1223 Pitzer K. and Mayorga G. (1973) Thermodynamics of electrolytes .2. Activity
1224 and osmotic coefficients for strong electrolytes with one or both ions univalent.
1225 *Journal of Physical Chemistry* **77**, 2300–2308.
- 1226 Pitzer K., Peiper J. and Busey R. (1984) Thermodynamic properties of aqueous
1227 sodium-chloride solutions. *Journal of Physical and Chemical Reference Data*
1228 **13**, 1–102.
- 1229 Pitzer K.S. and Simonson J.M. (1986) Thermodynamics of multicomponent, mis-
1230 cible, ionic systems: theory and equations. *The Journal of Physical Chemistry*
1231 **90**, 3005–3009. doi:10.1021/j100404a042.
- 1232 Pitzer K.S. and Sterner S.M. (1994) Equations of state valid continuously from
1233 zero to extreme pressures for H₂O and CO₂. *The Journal of Chemical Physics*
1234 **101**, 3111–3116. doi:10.1063/1.467624.
- 1235 Powell R., Holland T.J.B. and Worley B. (1998) Calculating phase diagrams
1236 involving solid solutions via non-linear equations, with examples using
1237 THERMOCALC. *Journal of Metamorphic Geology* **16**, **4**, 577–588. doi:
1238 10.1111/j.1525-1314.1998.00157.x.
- 1239 Quist A.S. and Marshall W.L. (1968) Electrical conductances of aqueous sodium

- 1240 chloride solutions from 0 to 800°C and at pressures to 4000 bars. *Journal of*
1241 *Physical Chemistry* **72**, 684–703. doi:10.1021/j100848a050.
- 1242 Rumpf B., Nicolaisen H., Ocal C. and Maurer G. (1994) Solubility of carbon diox-
1243 ide in aqueous solutions of sodium chloride: Experimental results and Correla-
1244 tion. *Journal of Solution Chemistry* **23**, 431–448.
- 1245 Sander W. (1912) On the solubility of carbon acid in water and some other solu-
1246 tions under high pressure. *Zeitschrift Fur Physikalische Chemie–Stoichiometrie*
1247 *Und Verwandtschaftslehre* **78**, 513–549.
- 1248 Santosh M. and Omori S. (2008) CO₂ flushing: A plate tectonic perspective.
1249 *Gondwana Research* **13**, 86 – 102. doi:10.1016/j.gr.2007.07.003.
- 1250 Sawamura S., Egoshi N., Setoguchi Y. and Matsuo H. (2007) Solubility of sodium
1251 chloride in water under high pressure. *Fluid Phase Equilibria* **254**, 158 – 162.
1252 doi:10.1016/j.fluid.2007.03.003.
- 1253 Seidell A. (1940) *Solubilities of inorganic and metal organic compounds*. DVan
1254 Nostrand Company, New York.
- 1255 Servio P. and Englezos P. (2001) Effect of temperature and pressure on the solu-
1256 bility of carbon dioxide in water in the presence of gas hydrate. *Fluid Phase*
1257 *Equilibria* **190**, 127 – 134. doi:10.1016/S0378-3812(01)00598-2.
- 1258 Sharygin A.V., Wood R.H., Zimmerman G.H. and Balashov V.N. (2002) Multi-
1259 ple Ion Association versus Redissociation in Aqueous NaCl and KCl at High
1260 Temperatures. *The Journal of Physical Chemistry B* **106**, 7121–7134. doi:
1261 10.1021/jp013647u.

- 1262 Shedlovsky T. (1938) The computation of ionization constants and limiting con-
1263 ductance values from conductivity measurements. *Journal of the Franklin In-*
1264 *stitute* **225**, 739 – 743. doi:10.1016/S0016-0032(38)90931-7.
- 1265 Sherman D.M. and Collings M.D. (2002) Ion association in concentrated NaCl
1266 brines from ambient to supercritical conditions: results from classical molec-
1267 ular dynamics simulations. *Geochemical Transactions* **3**, 102–107. doi:
1268 10.1186/1467-4866-3-102.
- 1269 Spear F. (1993) *Metamorphic Phase Equilibria and Pressure-Temperature-Time*
1270 *Paths*. Mineralogical Society of America, Washington, D. C.
- 1271 Spycher N., Pruess K. and Ennis-King J. (2003) CO₂-H₂O mixtures in the geolog-
1272 ical sequestration of CO₂. I. Assessment and calculation of mutual solubilities
1273 from 12 to 100°C and up to 600 bar. *Geochimica et Cosmochimica Acta* **67**,
1274 3015 – 3031. doi:10.1016/S0016-7037(03)00273-4.
- 1275 Sterner S. and Bodnar R. (1991) Synthetic fluid inclusions.X: Experimental de-
1276 termination of P-V-T-X properties in the CO₂-H₂O system to 6 kb and 700 °C.
1277 *American Journal of Science* **291**, 1–54.
- 1278 Sterner S. and Pitzer K. (1994) An Equation Of State For Carbon-Dioxide Valid
1279 From Zero To Extreme Pressures. *Contributions to Mineralogy and Petrology*
1280 **117**, 362–374.
- 1281 Stewart P.B. and Munjal P.K. (1970) Solubility of carbon dioxide in pure water,
1282 synthetic sea water, and synthetic sea water concentrates at -5deg. to 25deg. and
1283 10- to 45-atm. pressure. *Journal of Chemical & Engineering Data* **15**, 67–71.
1284 doi:10.1021/je60044a001.

- 1285 Surdo A.L., Alzola E.M. and Millero F.J. (1982) The (p, V, T) properties of
1286 concentrated aqueous electrolytes I. Densities and apparent molar volumes of
1287 NaCl, Na₂SO₄, MgCl₂, and MgSO₄ solutions from 0.1 molkg⁻¹ to saturation
1288 and from 273.15 to 323.15 K. *The Journal of Chemical Thermodynamics* **14**,
1289 649 – 662. doi:10.1016/0021-9614(82)90080-5.
- 1290 Takenouchi S. and Kennedy G. (1965) Solubility of carbon dioxide in NaCl so-
1291 lutions at high temperatures and pressures. *American Journal of Science* **263**,
1292 445–454.
- 1293 Takenouchi S. and Kennedy G.C. (1964) The binary system H₂O-CO₂ at high
1294 temperatures and pressures. *American Journal of Science* **262**, 1055–1074.
- 1295 Tatsumi Y. (1989) Migration of fluid phases and genesis of basalt magmas in
1296 subduction zones. *Journal of Geophysical Research* **94**, 4697–4707. doi:
1297 10.1029/JB094iB04p04697.
- 1298 Teng H., Yamasaki A., Chun M.K. and Lee H. (1997) Solubility of liquid CO₂
1299 in water at temperatures from 278 K to 293 K and pressures from 6.44 MPa to
1300 29.49 MPa and densities of the corresponding aqueous solutions. *The Journal*
1301 *of Chemical Thermodynamics* **29**, 1301 – 1310. doi:10.1006/jcht.1997.0249.
- 1302 Thompson A. (1992) Water in the Earth's upper mantle. *Nature* **358**, 295–302.
1303 doi:10.1038/358295a0.
- 1304 Thompson J.B.J. (1967) *Thermodynamic properties of simple solutions*. John Wi-
1305 ley and Sons, New York.
- 1306 Tipper E., Galy A., Gaillardet J., Bickle M., Elderfield H. and Carder E. (2006)
1307 The magnesium isotope budget of the modern ocean: Constraints from riverine

- 1308 magnesium isotope ratios. *Earth and Planetary Science Letters* **250**, 241 – 253.
1309 doi:10.1016/j.epsl.2006.07.037.
- 1310 Todheide K. and Franck E.U. (1963) Das Zweiphasengebiet die kritische Kurve
1311 im System Kohlendioxid-Wasser bis zu Drucken von 3500 bar. *Zeitschrift für*
1312 *Physikalische Chemie (Neue Folge)* **37**, 387 – 401.
- 1313 Vidal O. and Dubacq B. (2009) Thermodynamic modelling of clay dehydra-
1314 tion, stability and compositional evolution with temperature, pressure and
1315 H₂O activity. *Geochimica et Cosmochimica Acta* **73**, 6544 – 6564. doi:
1316 10.1016/j.gca.2009.07.035.
- 1317 Vilcu R. and Gainar I. (1967) Löslichkeit Der Gase Unter Druck In Flüssigkeiten
1318 .I. Das System Kohlendioxid-Wasser. *Revue Roumaine de Chimie* **12**, 181–189.
- 1319 White R., Powell R. and Holland T. (2001) Calculation of partial melting
1320 equilibria in the system Na₂O-CaO-K₂O-FeO-MgO-Al₂O₃-SiO₂-H₂O (NCKF-
1321 MASH). *Journal of Metamorphic Geology* **19**, 139–153. doi:10.1046/j.0263-
1322 4929.2000.00303.x.
- 1323 Wiebe R. and Gaddy V.L. (1939) The Solubility in Water of Carbon Dioxide at
1324 50, 75 and 100°C, at Pressures to 700 Atmospheres. *Journal of the American*
1325 *Chemical Society* **61**, 315–318.
- 1326 Wiebe R. and Gaddy V.L. (1940) The Solubility of Carbon Dioxide in Water at
1327 Various Temperatures from 12 to 40°C and at Pressures to 500 Atmospheres.
1328 Critical Phenomena. *Journal of the American Chemical Society* **62**, 815–817.

- 1329 Wigley M., Kampman N., Dubacq B. and Bickle M.J. (2012) Fluid-mineral reac-
1330 tions and trace metal mobilization in an exhumed natural CO₂ reservoir, Green
1331 River, Utah. *Geology* **40**, 555–558. doi:10.1130/G32946.1.
- 1332 Wilkinson J.J. and Johnston J.D. (1996) Pressure fluctuations, phase separation,
1333 and gold precipitation during seismic fracture propagation. *Geology* **24**, 395–
1334 398. doi:10.1130/0091-7613(1996)024<0395:PFPSAG>2.3.CO;2.
- 1335 Wishaw B.F. and Stokes R.H. (1954) The Diffusion Coefficients and Conduc-
1336 tances of Some Concentrated Electrolyte Solutions at 25°C. *Journal of the*
1337 *American Chemical Society* **76**, 2065–2071. doi:10.1021/ja01637a011.
- 1338 Yang S., Yang I., Kim Y. and Lee C. (2000) Measurement and prediction of phase
1339 equilibria for water+CO₂ in hydrate forming conditions. *Fluid Phase Equilibria*
1340 **175**, 75 – 89. doi:10.1016/S0378-3812(00)00467-2.
- 1341 Zakirov I., Sretenskaja N., Aranovich L. and Volchenkova V. (2007) Solubil-
1342 ity of NaCl in CO₂ at high pressure and temperature: First experimental
1343 measurements. *Geochimica et Cosmochimica Acta* **71**, 4251 – 4255. doi:
1344 10.1016/j.gca.2007.01.028.
- 1345 Zawisza A. and Malesinska B. (1981) Solubility of carbon-dioxide in liquid water
1346 and of water in gaseous carbon-dioxide in the range 0.2-5 MPa and at tempera-
1347 tures up to 473-K. *Journal of Chemical and Engineering Data* **26**, 388–391.
- 1348 Zelvinskii Y. (1937) Measurements of carbon dioxide solubility in water. (in Rus-
1349 sian). *Zhurn. Khim. Prom.* **14**, 1250–1257.

Symbol	Quantity
R	Ideal gas constant (= 8.314472 J.mol ⁻¹ .K ⁻¹)
T	Temperature
P	Pressure
STP	Standard temperature and pressure, 298.15K and 1 bar
T_C, x_C	Critical temperature and composition
μ_i	Chemical potential of end-member i
μ_i^0	Standard state chemical potential of i
x_i	Mole fraction of i
γ_i	Activity coefficient of i
a_i	Activity of i : $a_i = x_i \cdot \gamma_i$
σ_i^2	Variance of i
$\overline{G}_m^{\text{mix}}(x)$	Gibbs free energy of mixing
$\overline{G}_m(x)$	Gibbs free energy of the mixture
$\overline{G}_m^{\text{xs}}(x)$	Excess Gibbs free energy of the mixture
Φ_i	Proportion of i adjusted to a size parameter
W_{ij}^*	Interaction energy between i and j adjusted to a size parameter
W_j	Interaction energy between i and j
α_i	Size parameter for i
W_G, W_H, W_S, W_V	Interaction parameters on the Gibbs free energy, enthalpy, entropy and volume of mixing, respectively.
Λ_e, Λ_e	Equivalent conductance, respectively experimentally-determined and hypothetical from a completely dissociated electrolyte
Λ_e^0	Limiting equivalent conductance
η, η_0	Viscosity, respectively of the solution and of the pure solvent
ρ	Density of the solution
ϵ	Dielectric constant of water
\hat{a}	Ion size parameter 69

Table 1: Key to symbols used in the text.

Reference	Pressure - temperature range
Adams (1931)	25°C, 1-4 kbar
Compilation of data from Seidell (1940)	20-300°C, 1-4 kbar
Keevil (1942)	180-650°C, water vapor pressure
Clyne et al. (1981)	26-94°C, 1 bar
Farelo et al. (1993)	20-80°C, 1 bar
Pinho and Macedo (2005)	25-80°C, 1 bar
Sawamura et al. (2007)	20-40°C, 1-3 kbar

Table 2: Selected experimental results of halite solubility.

P bars	T °C	molality CO ₂	ρ_{Meas}	ρ_{Calc}	Deviation ‰
10	25	0.155	996.9	970.7	26.2
200	25	0.155	1005.3	1005.0	0.3
200	50	0.155	996.0	996.5	-0.5
200	100	0.155	966.5	965.8	0.7
200	150	0.155	926.4	926.7	-0.4
200	200	0.155	875.9	879.1	-3.7
200	250	0.185	813.4	821.0	-9.4
200	300	0.155	731.1	740.2	-12.4
280	350	0.155	631.7	642.1	-16.4
350	25	0.155	1011.7	1011.4	0.3
350	50	0.155	1002.2	1002.4	-0.2
350	100	0.155	973.1	973.9	-0.8
350	150	0.155	934.1	934.7	-0.6
350	200	0.155	885.9	887.2	-1.4
350	250	0.185	827.7	831.3	-4.4
350	300	0.155	754.7	760.6	-7.8
197	10	1.741	1020.8	1016.4	-4.2
246	10	1.796	1021.7	1020.5	-1.2
295	10	1.840	1024.0	1023.0	-1.0
197	15	1.702	1019.7	1015.8	-3.8
246	15	1.757	1021.0	1019.6	-1.3
295	15	1.801	1022.9	1022.0	-0.9
197	20	1.614	1017.7	1015.0	-2.7
246	20	1.675	1019.1	1019.0	-0.1
295	20	1.719	1019.8	1021.4	1.6

Table 3: Comparison of measured (ρ_{Meas}) and calculated (ρ_{Calc}) densities at various pressures, temperatures and CO₂ concentrations. Measurements at CO₂ concentrations around 0.15 M originate from Hnedkovský et al. (1996), and measurements above 1M CO₂ are taken from Teng et al. (1997).

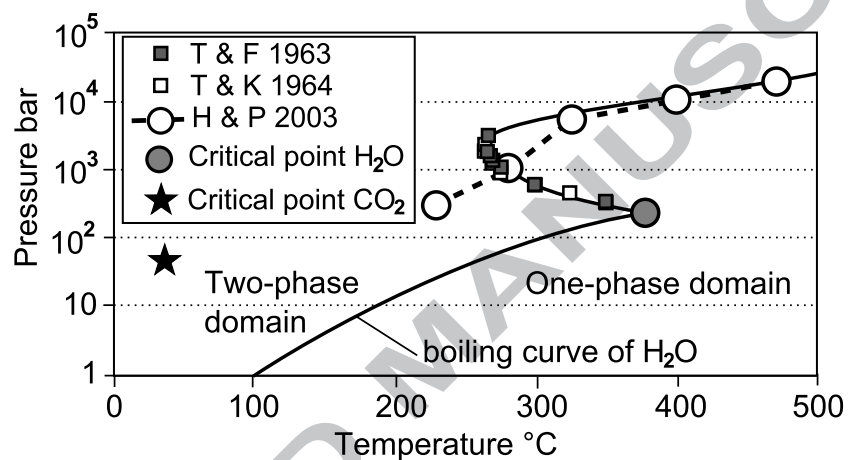


Figure 1: Phase diagram for CO₂-H₂O mixtures. Note that pressure is on a logarithmic scale. T&F 1963: Measurements of Todheide and Franck (1963). T&K1964: Measurements of Takenouchi and Kennedy (1964). H&P 2003: Model of Holland and Powell (2003). High pressure - low temperature solid phases (ices and clathrates) are not represented.

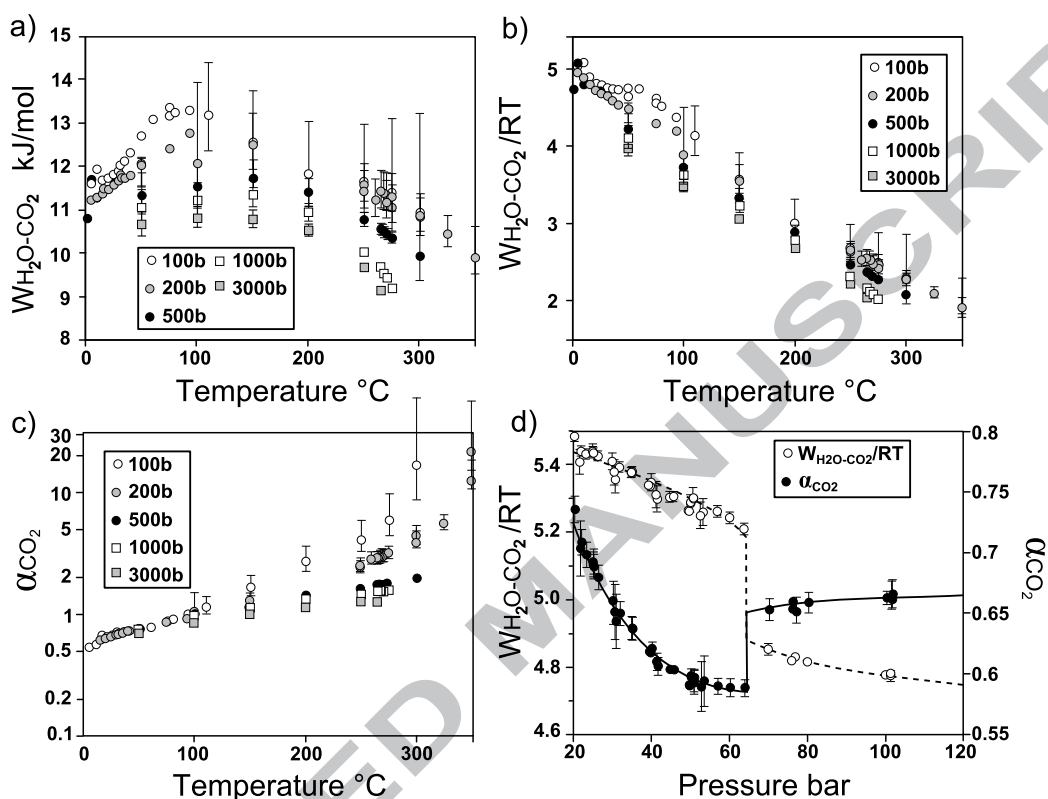


Figure 2: Representative values of $W_{H_2O-CO_2}$ and a_{CO_2} from selected experimental results. a) and b) respectively show isobaric values of $W_{H_2O-CO_2}$ and $W_{H_2O-CO_2}/RT$ as a function of temperature. c) Isobaric values of a_{CO_2} as a function of temperature. Note the log scale to represent low pressure value of a_{CO_2} . d) Variations of $W_{H_2O-CO_2}$ (open symbols and dashed lines) and a_{CO_2} (closed symbols and plain lines) with pressure at 25°C. A step is seen at the boiling curve of CO₂. Lines are calculated with eq. 8 and 9. Uncertainties are smaller than the size of the point when not indicated.

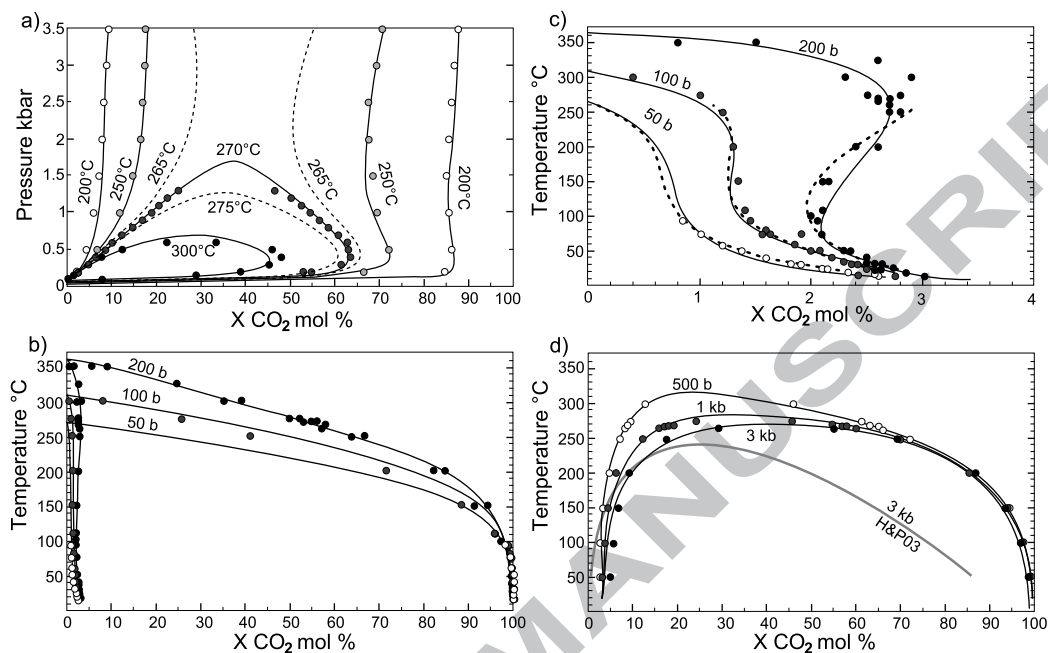


Figure 3: Phase equilibrium in the H₂O-CO₂ system at various pressures and temperatures (cross-sections through figure 1). Lines are calculated and points are experimental results at the pressure - temperature corresponding to the lines closest to which they plot. a) Pressure-composition phase diagram at different temperatures. The solvus closes at low pressure against the boiling curve of water ($X \text{ CO}_2 = 0$). Dashed lines illustrate the dependency of the phase diagram to temperatures around 270°C. Corresponding experimental measurements are not indicated for clarity. b), c) and d) show temperature-composition phase diagrams at different pressures. c) is a close-up view of b) for the water-rich phase. Dotted lines are calculated with the model of Duan and Sun (2003). The thick gray line in d) is calculated with the parameters of Holland and Powell (2003) plotted in figure 13.

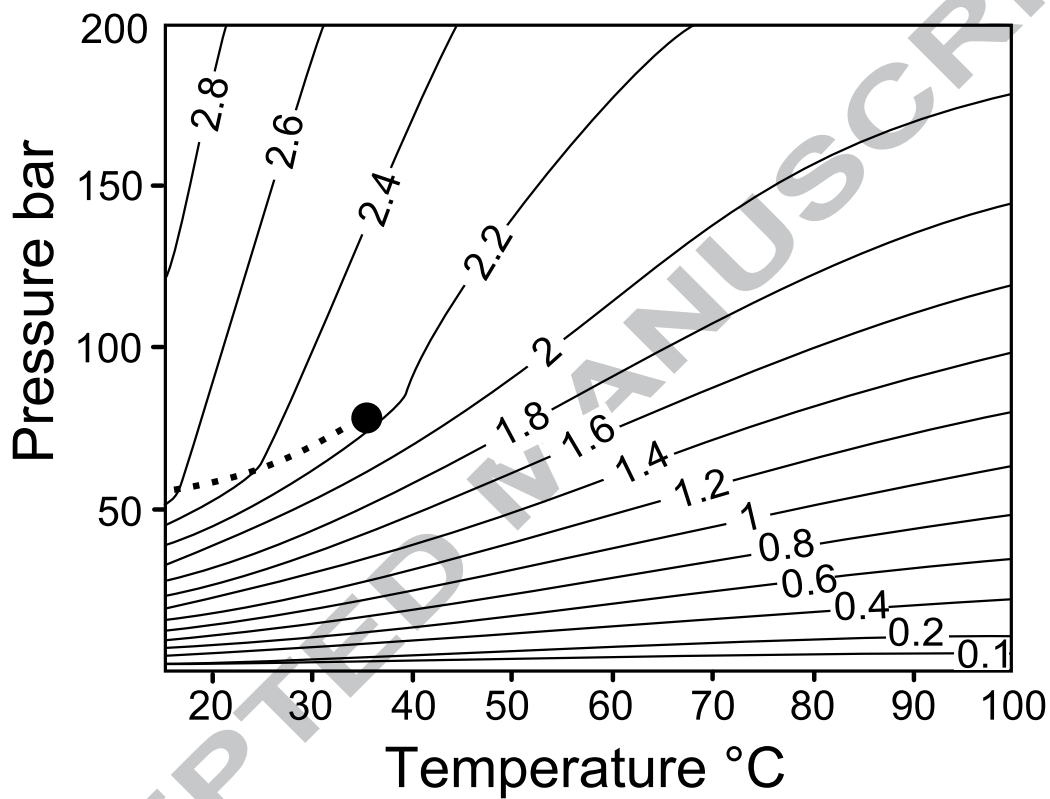


Figure 4: a) Isopleths of calculated CO₂ solubility (mol. %) in pure water at low pressures and temperatures. The dark circle indicates the critical point of CO₂ and the dashed line is the liquid-gas transition of CO₂.

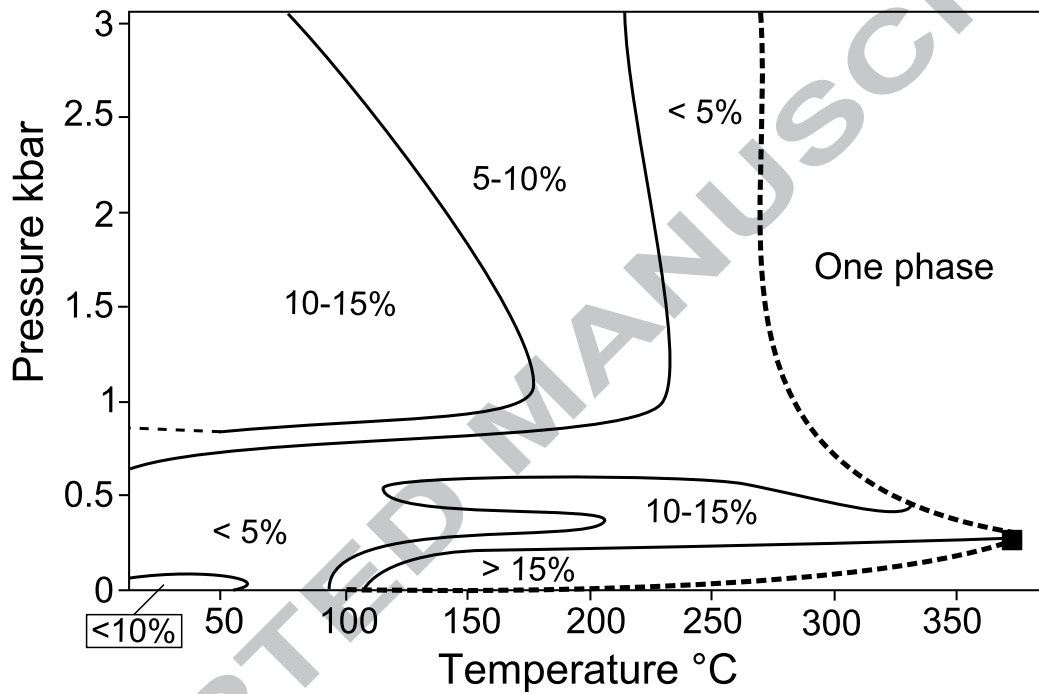


Figure 5: Map of uncertainties on CO₂ solubility, in percent of the calculated value. This map takes into account experimental uncertainties and the misfit of the model to the data.

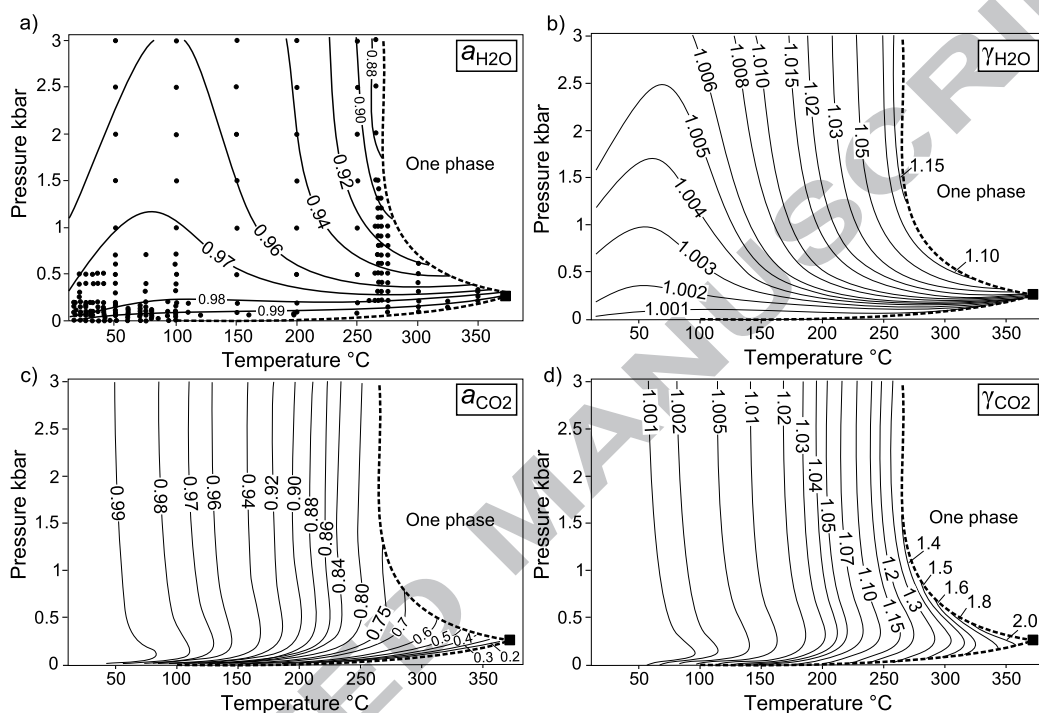


Figure 6: Isopleths of calculated a) water activity ($a_{\text{H}_2\text{O}}$) and b) water activity coefficient ($\gamma_{\text{H}_2\text{O}}$) in CO₂-saturated solutions, c) CO₂ activity (a_{CO_2}) and d) CO₂ activity coefficient (γ_{CO_2}) in the water-saturated CO₂-rich phase, between 25 and 380°C and 1 bar to 3 kbar. Dashed curves illustrate the two critical mixing lines. Points in a) represent pressure-temperature conditions of experimental results used in this study. The square indicates the critical point of water.

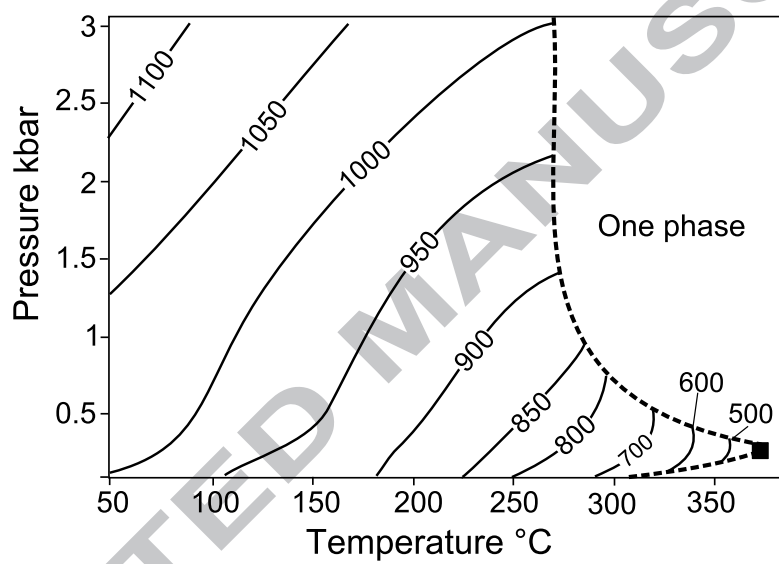


Figure 7: Calculated density isopleths of the CO₂-saturated aqueous phase over the range 0.1-3kb and 50-370°C, in kg.m⁻³.

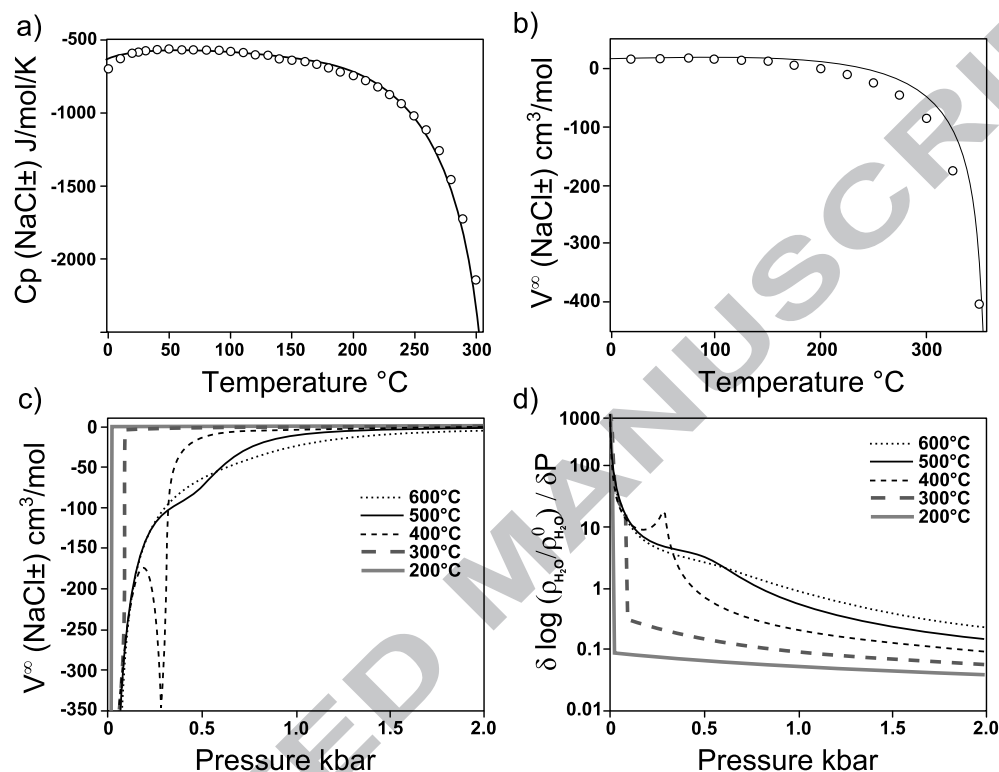


Figure 8: Heat capacity (C_p) and volume of NaCl± at infinite dilution (V^∞) calculated with the modified density model (Holland and Powell, 1998). a) Heat capacity at 200 bars compared to measurements from Pitzer et al. (1984). b) Comparison with the experimentally-derived volumes of Grant-Taylor (1981) and L'Vov et al. (1981). c) Isotherms of calculated V^∞ (NaCl±) up to 2 kbars. d) Isotherms of the pressure derivative of $\ln(\rho_{\text{H}_2\text{O}}/\rho_{\text{H}_2\text{O}}^0)$, plotted on a log scale and used in the calculation of V^∞ (NaCl±).

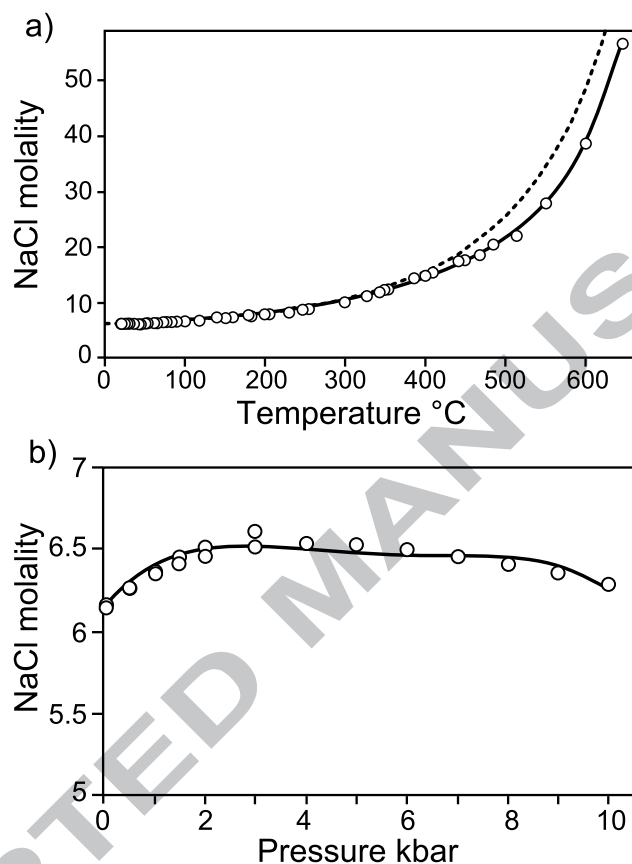


Figure 9: a) Solubility of halite calculated as a function of temperature with the model of Mao and Duan (2008, dotted line) and with the present model (bold line). The solubility is calculated at water vapor pressure below the critical point of water and along a linear pressure gradient linking experimental pressures above the critical point of water. b) Solubility of halite calculated at 25°C as a function of pressure. Points are experimental measurements indicated in table 2.

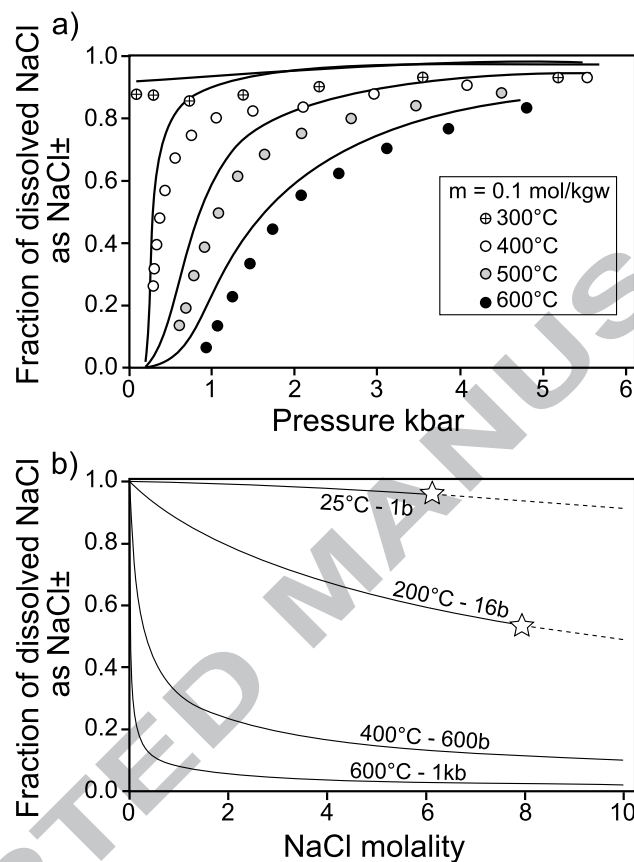


Figure 10: a) Fraction of dissociated aqueous NaCl ($x_{\text{NaCl}\pm}$) as a function of pressure, calculated at different temperatures and compared to the degree of association calculated from the conductivity measurements of Quist and Marshall (1968) at 0.1 molal, as described in the text. b) $x_{\text{NaCl}\pm}$ calculated as a function of the total concentration of NaCl for various pressures and temperatures. The fraction of NaCl⁰ is $x_{\text{NaCl}^0} = 1 - x_{\text{NaCl}\pm}$. Stars indicate halite saturation.

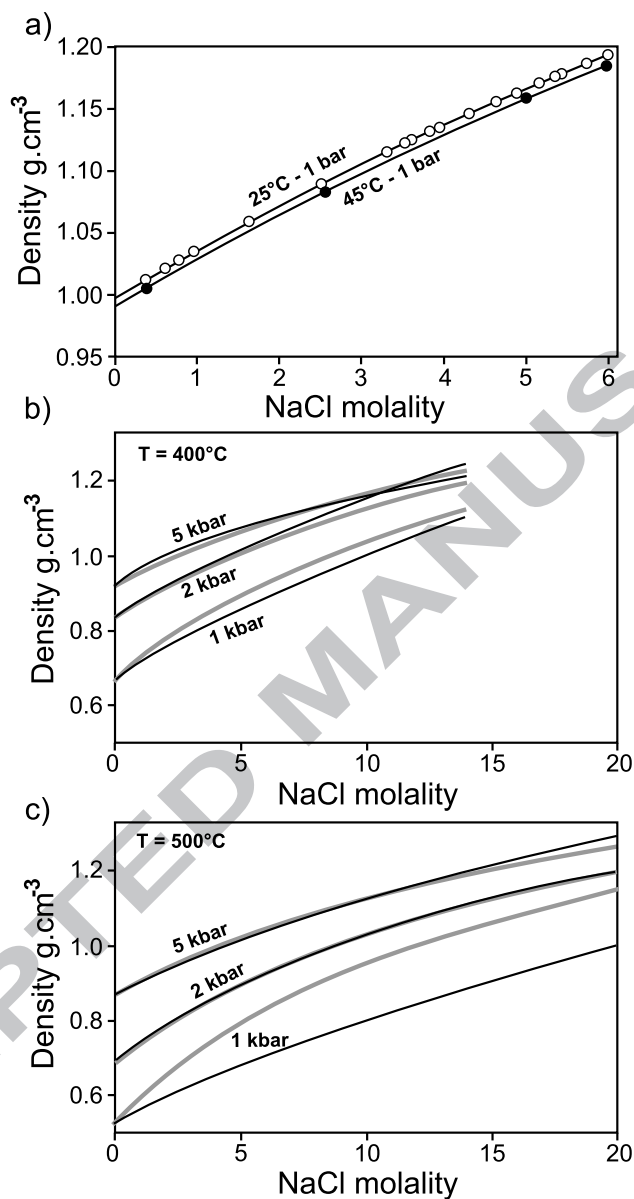


Figure 11: a) Density of NaCl solutions calculated at 1 bar (dark line) compared to the measurements of Surdo et al. (1982) at 25°C (open symbols) and 45°C (closed symbols). b) and c): density of NaCl solutions calculated at 400 and 500 °C for various pressures with this model (dark lines) and with the model of Driesner (2007) (thick gray lines).

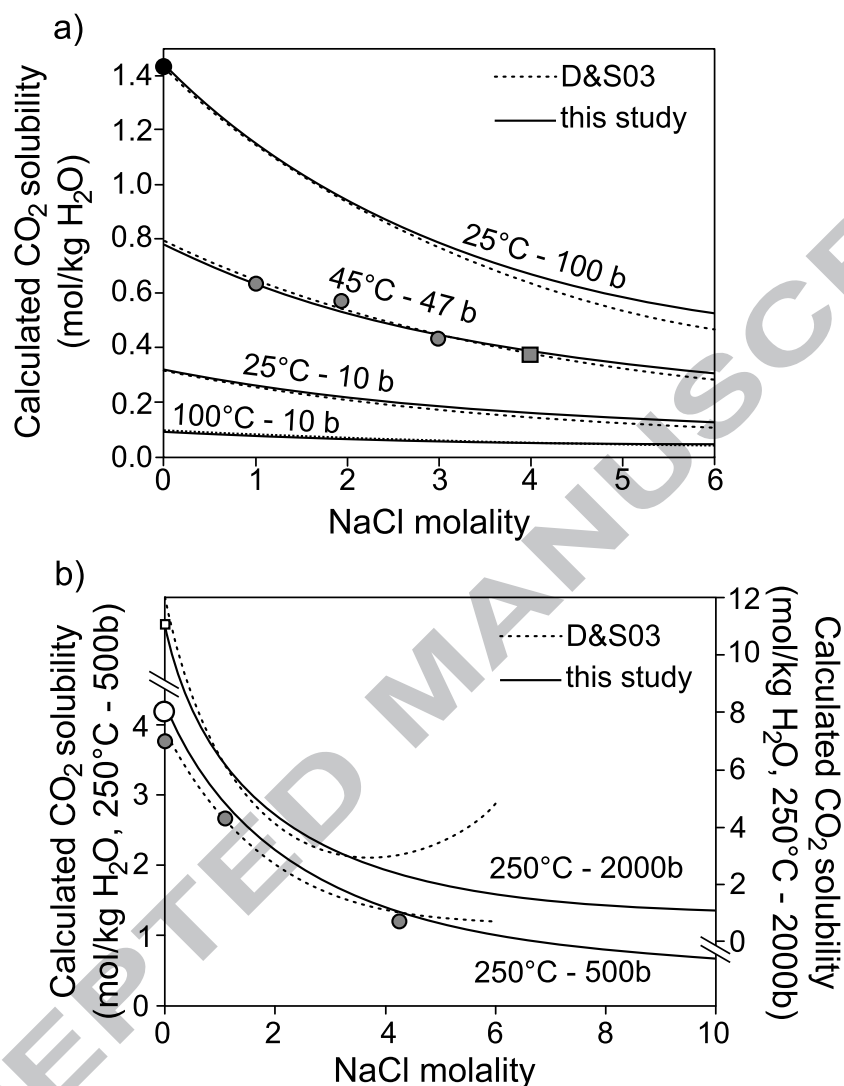


Figure 12: a) Solubility of CO₂ as a function of concentration of NaCl, calculated at indicated pressure and temperatures with the present model and Duan and Sun (2003, dotted line labeled D&S03). Black circle at 25°C: Wiebe and Gaddy (1940). Grayed symbols are measurements of Drummond (1981) between 47 and 48 bars (circles) and at 42 bars (square). b) CO₂ solubility at 250°C calculated at 500 bars (left axis) and 2000 bars (right axis). Grayed circles are measurements of Takenouchi and Kennedy (1965) with unknown uncertainties. Open symbols are measurements of Todheide and Franck (1963) at 500 bars (circle) and 2000 bars (square), whose sizes indicate experimental uncertainty.

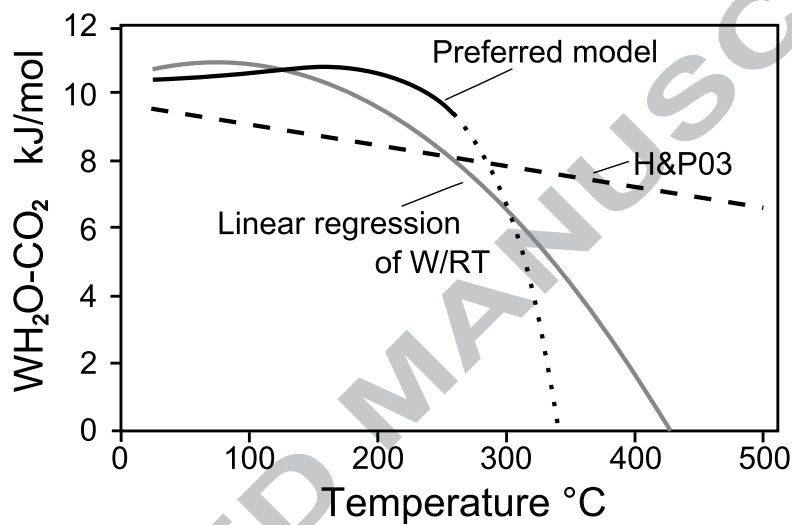


Figure 13: Comparison of values for $W_{\text{H}_2\text{O}-\text{CO}_2}$ at 3 kbar given by the model of Holland and Powell (2003, dashed line), by linear regression of $W_{\text{H}_2\text{O}-\text{CO}_2}/RT$ (gray line, see section 2.2) and by the model proposed in this study, in the two-phase domain (plain line) and extrapolated in the one-phase domain (dotted line).